




Mean-field-derived IBM-1 Hamiltonian with intrinsic triaxial deformation

Polytimos Vasileiou ^{1,*}, Dennis Bonatsos ², and Theo J. Mertzimekis ¹

¹*Department of Physics, National & Kapodistrian University of Athens, Zografou Campus, GR-15784, Greece*

²*Institute of Nuclear and Particle Physics, National Center for Scientific Research “Demokritos”, GR-15310, Aghia Paraskevi, Greece*



(Received 17 April 2024; accepted 13 June 2024; published 8 July 2024)

An interacting-boson-model-1 (IBM-1) Hamiltonian, derived from self-consistent mean-field calculations using a Skyrme energy density functional is employed for the study of energy spectra and $B(E2)$ transition strengths in the even-even $^{162-184}\text{Hf}$ and $^{168-186}\text{W}$. An intrinsic triaxial deformation, derived from fermionic proxy-SU(3) irreps, is incorporated into the IBM-1 potential energy curve, which is subsequently mapped to the fermionic one, in order to derive the parameters of the IBM-1 Hamiltonian. It is shown that the inclusion of the intrinsic triaxial deformation derived from the proxy-SU(3) irreps leads to a significantly improved agreement between the theoretical predictions and experimental data for the low-lying quadrupole bands in the examined isotopes, without the need of higher-order terms in the IBM-1 Hamiltonian. The calculated $B(E2)$ transition strengths are also improved, compared to the axially symmetric case. The recently suggested preponderance of triaxial deformation over extended regions of the nuclear chart is obtained as a byproduct. Future potential improvements and extensions to this mapping approach are also discussed.

DOI: [10.1103/PhysRevC.110.014313](https://doi.org/10.1103/PhysRevC.110.014313)

I. INTRODUCTION

The nuclear shell model [1–3] is widely considered to provide a detailed microscopic description of atomic nuclei in terms of their constituent protons and neutrons. The spherical shell model [1] is based on the isotropic three-dimensional harmonic oscillator, possessing the SU(3) symmetry [4–6], to which the spin-orbit force is added, which destroys the SU(3) symmetry beyond the sd shell. In most cases only the valence protons and valence neutrons outside spherical closed shells are taken into account, in order to reduce the computational demands, although recently no-core shell model approaches [7–9] are being developed for light nuclei.

An alternative description of the collective properties of atomic nuclei is provided by the macroscopic collective model of Bohr and Mottelson [10–12], in which nuclear shapes are described in terms of the collective variables β and γ , corresponding to the departure from sphericity and to the departure from axial symmetry, respectively.

A severe truncation of the shell model space in even-even nuclei is provided by the phenomenological interacting boson model (IBM) [13], having an overall U(6) symmetry, in which the collective properties of medium-mass and heavy nuclei are described in terms of s and d bosons, possessing angular momentum 0 and 2, respectively. These bosons correspond to correlated fermion pairs, equal in number to the valence proton pairs and valence neutron pairs, measured from the nearest closed shell. Only one- and two-body interactions among the bosons are taken into account. Three dynamical symmetries exist in IBM: U(5) [14], SU(3) [15],

and O(6) [16], corresponding to vibrational (near-spherical), axially deformed, and soft to triaxial deformation (called γ -unstable) nuclei, respectively. In the original version of the model, called IBM-1, no distinction is made between bosons corresponding to valence protons and neutrons. When this distinction is made, IBM-2 occurs. In the classical limit of IBM [17–19], built through the use of coherent states (also called intrinsic states [13]), potential energy surfaces (PESs) corresponding to IBM Hamiltonians are obtained in terms of the collective variables β and γ .

Along a different path, self-consistent mean-field many-body methods have been developed for atomic nuclei, using nonrelativistic interactions [20–22] or relativistic energy density functionals [23–25]. PESs are readily constructed within this framework for nuclei of any mass, but the calculation of spectra and electromagnetic transition rates becomes demanding.

A bridge between the mean field and IBM approaches has been built by Nomura *et al.* [26–28]. Along this path, the PES derived from the mean-field calculations is used to determine the free parameters appearing in IBM, by fitting the IBM PES to the mean-field PES. In this way one can subsequently use the IBM codes [29] to derive predictions for spectra and electromagnetic transition rates for specific nuclei without having to fit any free parameters to the data of each individual nucleus, as was done in the early days of IBM. In other words, one is able to obtain detailed spectroscopic predictions for a specific nucleus from an IBM Hamiltonian with microscopically derived parameters.

On the other hand, triaxiality in even-even nuclei [30–32] has been attracting recently considerable attention. While the number of nuclei in which triaxiality is dominant is rather small, as indicated by the experimental odd-even staggering

*Contact author: polvasil@phys.uoa.gr

within their γ bands [33,34], it has been recently pointed out that some degree of triaxiality is present almost everywhere on the nuclear chart [35–37].

It is known that within the standard IBM-1, in which only one- and two-body interactions are included, no triaxial shapes are obtained [38]. Triaxial shapes can be obtained by taking into account three-body terms [38–41]. An alternative path is to use the standard IBM-2 with only one- and two-body interactions, in which distinction between protons and neutrons is made. Triaxial shapes then occur when valence protons are particles and valence neutrons are holes, or vice versa [42]. In the SU(3) framework of IBM, particles are described by prolate irreducible representations (irreps) of the type $(N_1, 0)$, while holes are described by oblate irreps of the form $(0, N_2)$. Combining these irreps one gets for the whole nucleus the irrep (N_1, N_2) , which is triaxial. This approach has been called the SU(3)* limit of IBM-2 [42–44].

In the present work we propose an alternative path for the description of triaxiality in IBM-1, insisting on the use of one- and two-body interactions only but introducing an intrinsic triaxial deformation of microscopic origin. The value of the intrinsic triaxial deformation is obtained through the proxy-SU(3) approximation [45–47] to the shell model, described below. The parameters of the IBM-1 Hamiltonian are obtained by fitting its PES to the PES obtained from mean-field calculations employing the Skyrme energy density functional [48]. The present approach resembles the method of Nomura *et al.* [26,27] with two main differences: a) the use of an intrinsic triaxial deformation in the present case, and b) the use of different energy density functionals. While the latter difference is not expected to inflict major changes, since all energy density functionals in use are known to provide good results, the first one should reveal substantial differences, to be estimated through comparison of the present results to earlier approaches [49–51].

Discussion on the microscopic origin of the intrinsic triaxial deformation to be used within IBM-1 is now in place.

A bridge between the spherical shell model and nuclear deformation has been built by Elliott [52–54], who pointed out that the wave functions in a degenerate oscillator level, classified according to the irreps of SU(3), for which the symbol (λ, μ) is used [52], can be expressed as integrals of the Hill-Wheeler type over intrinsic states, and furthermore that all states belonging in a band involve the same intrinsic state in the integral [53] with states in a band having all other quantum numbers equal being distinguished by an additional quantum number K [the “missing quantum number” in the decomposition from SU(3) to SO(3)]. As a consequence, simple expressions are obtained for the quadrupole moments, which resemble those of a rotational model with permanent deformation. In other words, Elliott revealed deformation within the spherical shell model.

Elliott’s SU(3) symmetry is destroyed in shells beyond the sd shell, because the spin-orbit interaction pushes down in energy the orbitals of each shell bearing the highest total angular momentum j [1]. As a consequence a shell beyond the sd one consists of its initial orbitals, minus the deserting orbitals (those with the highest j , which went to the shell below), plus the intruder orbitals coming from the shell above (in which

they were having the highest j). The proxy-SU(3) approximation for even-even nuclei [45–47] proved that a unitary transformation [55] allows the replacement of the intruder orbitals (except the single level with the highest projection of j) by the deserting orbitals, thus reestablishing the SU(3) symmetry of the shell, with the exception of the left-over single level, which however is found to lie highest in energy, thus not influencing most nuclei in the shell. The validity of the proxy-SU(3) symmetry has been first proved [45,56] within the Nilsson’s deformed shell model [57,58], while later its connection to the spherical shell model has also been clarified [55].

In proxy-SU(3) symmetry the SU(3) irreps to which the valence protons and the valence neutrons correspond are used, labeled by (λ_p, μ_p) and (λ_n, μ_n) , respectively, coupled to the most stretched irrep $(\lambda, \mu) = (\lambda_p + \lambda_n, \mu_p + \mu_n)$ [46]. What is of utmost importance is that for each kind of nucleons the highest weight irrep is used, which is the most symmetric one [59], as required by the Pauli principle and the short-range nature of the nucleon-nucleon interaction, as discussed in detail in Refs. [46,59]. It should be noticed that the highest weight irrep is identical to the irrep possessing the highest eigenvalue of the second order Casimir operator of SU(3), related to the quadrupole-quadrupole interaction, up to the middle of the shell, but this is not the case any more beyond midshell, as it can be seen in Table I of Ref. [46].

The Elliott labels λ and μ are known to be connected to the shape variables β and γ of the collective model, this connection being achieved by mapping the eigenvalues of the invariant operators of the two theories [60,61]. Using this mapping from the (λ, μ) irrep characterizing a nucleus, parameter-independent predictions for its deformation variable β and its axial symmetry variable γ are obtained [46], providing among other results an explanation for the dominance of prolate over oblate shapes [62,63] in the ground states of even-even nuclei, as well as an argument in favor of the recently suggested preponderance of triaxiality in heavy deformed nuclei [35–37] supported by empirical evidence, provided by the experimental ratio of the band head of the γ band over the first excited state of the ground state band, $E(2_{\gamma}^+)/E(2_g^+)$ [64], through use of the triaxial rotor model [30,65,66], as seen in Sec. VI of [46].

Medium-mass and heavy deformed nuclei are described in IBM-1 within its SU(3) dynamical symmetry [13,15], in which the ground state band belongs to the SU(3) irrep $(2N_B, 0)$, where N_B is the number of bosons corresponding to the specific nucleus. Since in this irrep one has $\mu = 0$, the value of γ is also close to zero. This is not the case in the proxy-SU(3) scheme, in which almost all nuclei have $\mu \neq 0$, as seen for example in Tables II and III of Ref. [46]. This means that γ can obtain values away from zero, in agreement with the experimental expectations, as seen in Figs. 5 and 6 of Ref. [46]. It is therefore reasonable to consider an IBM description of medium-mass and heavy nuclei assuming an intrinsic nonzero value of γ . The Hf and W series of isotopes provide an appropriate test-ground for this assumption, since data exist for several isotopes extending from moderate to strong deformations [64].

It should be noticed that in IBM-1 the ground state band (gsb) sits alone in the $(2N_B, 0)$ SU(3) irrep, while the γ

($K = 2$) and β ($K = 0$) bands lie in the next irrep, ($2N_B - 4, 2$) [13,15]. As a consequence, no $B(E2)$ transitions are allowed to connect the γ band to the gsb, since they belong to different irreps, which cannot be connected by the quadrupole operator, which is a generator of SU(3), thus the SU(3) symmetry has to be broken [67], since the experimental $B(E2)$ s connecting the γ band to the gsb are known to be substantial [64]. This problem is avoided in the proxy-SU(3) scheme, since the gsb and the γ band belong to the same irrep with $\mu \neq 0$, thus no *a priori* need for breaking the SU(3) symmetry arises. The problem is known to be avoided also within the pseudo-SU(3) scheme [68–70], an alternative way of re-establishing the SU(3) symmetry of the three-dimensional harmonic oscillator in medium-mass and heavy nuclei.

In short, Elliott proved microscopically that deformation occurs within the spherical shell model based on an intrinsic state. In the present approach, we exploit the fact that the proxy-SU(3) irreps, dictated in a parameter-free way by the Pauli principle and the short range nature of the nucleon-nucleon interaction, exhibit non-vanishing values of the Elliott label μ , i.e., nonvanishing values of the collective variable γ , while in IBM-1 the SU(3) irreps containing the ground state band have $\mu = 0$, because of the bosonic nature of the constituent particles. By introducing an intrinsic nonvanishing value of γ in IBM-1, we therefore incorporate into the classical limit of IBM-1 the triaxiality feature required by the Pauli principle and the short-range nature of the nucleon-nucleon interaction.

In different words, Elliott, working within the microscopic spherical shell model, discovered an intrinsic state corresponding to departure from sphericity in the form of axial deformation, prolate or oblate. Within the microscopic spherical shell model the Pauli principle is explicitly taken into account, since protons and neutrons are used, which are fermions. In addition, the short-range nature of the nucleon-nucleon interaction is taken into account through the form of the harmonic oscillator potential. The question is how to handle departure from axial deformation, i.e., triaxial shapes, within the phenomenological IBM-1, in which the constituent particles are bosons, ignoring the Pauli principle, without adding higher order (cubic) terms, which would lead us beyond the original definition of IBM-1, and without introducing the distinction between protons and neutrons, which would lead us to IBM-2. The way proposed in the present approach is to start from the classical limit of IBM-1, formed with the use of coherent states, and add to it the triaxial deformation in the form of a nonvanishing value of the deformation variable γ . The specific value of γ is not treated as a free parameter, but is obtained in a parameter-free way from the proxy-SU(3) approximation to the shell model, in which both the Pauli principle and the short-range nature of the nucleon-nucleon interaction are explicitly taken into account, leading to the choice of the highest weight SU(3) irrep as the one describing the nucleus.

II. THEORETICAL PROCEDURE

We begin our analysis by performing constrained Skyrme Hartree-Fock + Bardeen-Cooper-Schrieffer (BCS)

(denoted HF + BCS, for the sake of brevity) calculations for each of the isotopes under study, with the constraint being placed on the quadrupole deformation parameter, β . We employ the SKYAX [48] code to carry out the energy density functional (EDF) calculations on a two-dimensional mesh on the r - z plane, where the mesh spacing of $dr = dz = 0.7$ fm is kept constant throughout. The SV-bas [71] EDF is used for the calculations. This functional is the starting point for the systematic variation (SV) set of parametrizations—a set of relatively modern parametrizations to the Skyrme interaction, which has reached a lot of success, being employed in various theoretical studies in recent years—and as such, it was chosen for our calculations (see also Ref. [72], and references therein, for a more detailed discussion on the SV family of EDFs). For the pairing, a density-dependent δ force was employed (see Ref. [48] for more details). However, it should be noted that, similar to the case of Refs. [26–28,49], the choice of Skyrme interaction does not essentially impact the results of the study, as long as the usual ones are considered. For each isotope, a set of constrained HF + BCS calculations is carried out for each value of β , leading to the construction of the corresponding potential energy curve (PEC). Since the total energy is used for the mapping procedure, all of the ingredients, including those related to kinetic terms, are supposed to be taken sufficiently into consideration [49].

Having obtained the HF + BCS PEC for each isotope, we move on to the IBM description of the PEC. The extended consistent Q formalism (ECQF) [73], first introduced in [74,75], is adopted to write the IBM-1 Hamiltonian in the form [76,77]

$$H(\zeta, \chi) = c \left[(1 - \zeta) \hat{n}_d - \frac{\zeta}{4N_B} \hat{Q}^x \hat{Q}^x \right], \quad (1)$$

where N_B is the number of valence bosons, $\hat{n}_d = d^\dagger \cdot \vec{d}$, $\hat{Q}^x = (s^\dagger \vec{d} + d^\dagger s) + \chi (d^\dagger \vec{d})^{(2)}$ the number operator for quadrupole bosons, and the quadrupole operator, respectively, and c is a scaling factor. The above Hamiltonian encompasses the entire IBM symmetry triangle [65,78,79], along with the U(5)–O(6)–SU(3) dynamical symmetry limits of the IBM, by making use of two structural parameters, ζ and χ . The parameters (ζ, χ) describing a nucleus can be placed in the IBM symmetry triangle by converting them into polar coordinates, through the relations [80,81]

$$\rho = \frac{\sqrt{3}\zeta}{\sqrt{3}\cos(\theta_\chi) - \sin(\theta_\chi)}, \quad \theta = \frac{\pi}{3} + \theta_\chi \quad (2)$$

with $\theta_\chi = (2/\sqrt{7})(\pi/3)\chi$.

Finally, the coherent state formalism [17,19,82] of the IBM is employed to extract the following expression for the energy surface, $E(\beta, \gamma)$, corresponding to the Hamiltonian of

Eq. (1) [83]:

$$E(\beta, \gamma) = \frac{cN_B\beta^2}{1+\beta^2} \left[(1-\zeta) - (\chi^2+1) \frac{\zeta}{4N_B} \right] - \frac{5c\zeta}{4(1+\beta^2)} - \frac{c\zeta(N_B-1)}{4(1+\beta^2)^2} \times \left[4\beta^2 - 4\sqrt{\frac{2}{7}}\chi\beta^3 \cos 3\gamma + \frac{2}{7}\chi^2\beta^4 \right]. \quad (3)$$

Equation (3) relates the structural parameters (χ, ζ) of the ECQF Hamiltonian with the (β, γ) classical coordinates linked to the Bohr geometrical variables [10,12,13]. More specifically, ζ is related to the axial quadrupole deformation parameter, β , while χ is associated with the triaxiality parameter, γ , which regulates the degree of triaxial deformation of a nucleus.

It should be noted that the deformation parameter of the boson system is not identical to that of the geometrical model, since the former is derived by taking into account only the valence bosons, in contrast to the latter, for which the entirety of the shell-model space is considered [18]. Thus, the IBM deformation parameter, β is always larger than the corresponding fermionic one, β_F , and, to a good approximation, one can assume $\beta \propto \beta_F$ [18]. One can then go on to write

$$\beta = C_\beta \beta_F \quad (4)$$

with $C_\beta (> 1)$ being the proportionality coefficient for the β deformation [26,51].

Regarding the triaxiality parameter of the bosonic PEC, as a first approach we assume axial deformations, and equate

$$\gamma_F = \gamma = 0^\circ. \quad (5)$$

By imposing the conditions (5) and (4) in Eq. (3), we obtain the boson potential energy curves for each of the studied isotopes, as functions of the axial quadrupole deformation, β , with parameters χ, ζ, c , and C_β , namely,

$$E(\beta, \gamma = 0) \rightarrow E(\beta) \equiv E(\beta_F; C_\beta, \chi, \zeta, c, N_B). \quad (6)$$

The procedure followed for the mapping of the IBM PECs to the EDF calculated ones, and the subsequent determination of the optimal set of IBM-1 parameters for each isotope, is outlined below.

The intervals $\chi = [-\sqrt{7}/2, 0]$ and $\zeta = [0, 1]$ are divided in steps, with fixed step-sizes $d\chi$ and $d\zeta$, and the same is done for C_β , for which the selected interval is [1,10]. The choice of the lower limit for C_β has already been justified by the discussion in the preceding paragraphs, while for the upper limit of this range, a sufficiently large value has been used, such that the C_β^{best} optimal value is enclosed in the defined interval. The choice of $C_\beta^{\text{max}} = 10$ seems to be sufficient, based on our results, as well as the results of similar studies on $^{166-180}\text{Hf}$ [51] and $^{182-194}\text{Hf}$ [49], where an IBM-2 Hamiltonian was mapped to Hartree-Fock-Bogoliubov (HFB) EDFs for calculations.

For each set of $(\chi^i, \zeta^i, C_\beta^i)$, an IBM PEC is generated through Eqs. (3) and (6), and compared to the HF PEC. The set of optimal (χ, ζ, C_β) parameters are chosen such that the best reproduction of the overall shape and curvature of

the HF PEC by the IBM PEC, up to a range of a few MeV from the absolute minimum of the microscopic PEC is achieved (Figs. 1 and 2).

The resulting χ and ζ values, along with the valence boson number, N_B , are then used as inputs for the diagonalization of the IBM-1 ECQF Hamiltonian of Eq. (1), carried out with the IBAR code by Casperson [29]. The scale, c , entering Eq. (1) to obtain quantitative results for the calculated energy levels, is chosen so as to reproduce the experimental $E(2_1^+)$ for each isotope.

The assumption of “pure” axial deformations ($\gamma = 0^\circ$) is enough to sufficiently reproduce the first few low-lying energy levels of the gsb of the studied nuclei (up to the 8_1^+ level, in most cases). However, the following discrepancies still persist:

- (i) The $R_{4/2} \equiv E(4_1^+)/E(2_1^+)$ ratios (see Table I and Figs. 3 and 4) are generally underestimated, compared to the experimental ones.
- (ii) The calculated gsb energy levels begin to diverge from the experimental ones, with increasing values of spin (Figs. 5(a) and 5(e)).
- (iii) The band spacings of the members of the β band are not accurately reproduced (Figs. 5(c) and 5(g)).
- (iv) The energy values for the γ band members are systematically underpredicted, while there is a pronounced odd-even staggering [i.e., $2_\gamma^+, (3_\gamma^+, 4_\gamma^+), (5_\gamma^+, 6_\gamma^+), \dots$] within the γ bands (Figs. 6(a) and 6(b)).

The resulting band levels for $^{162-184}\text{Hf}$ and $^{168-186}\text{W}$ are shown in Figs. 5(a), 5(c), 5(e), 5(g), and 6(a)–6(d) (see also Fig. 7(a) for an indicative level scheme). It is evident that this initial approach cannot provide a sufficiently accurate simultaneous description of the ground, β , and γ bands in the investigated members of the Hf and W isotopic chains.

Taking a closer look at the empirical values for the triaxiality parameter, γ , spanning the entire rare-earth region of the nuclear chart, it is observed that even for the most axially-symmetric nuclei, low, yet nonzero values of $\gamma \approx 8^\circ$ appear (this is discussed in [18,30,65,66,84], see also Fig. 5 of Ref. [46]). Thus, the incorporation of a degree of triaxiality, and the impact on the various bands follows as the next step in our calculations.

In the framework of the IBM-1, triaxiality can be achieved through the inclusion of higher order terms, such as three- and four-body terms of the form $(d^\dagger \times d^\dagger \times d^\dagger) \cdot (\tilde{d} \times \tilde{d} \times \tilde{d})$ [38,39], $(\hat{Q} \times \hat{Q} \times \hat{Q})$, $(\hat{L} \times \hat{Q} \times \hat{L})$ and $(\hat{L} \times \hat{Q}) \cdot (\hat{L} \times \hat{Q})$ [85,86]. An alternate path to triaxiality was undertaken in recent years, through the implementation of group-theoretical methods, utilizing SU(3) irreps (see, e.g., [85–89], and references therein).

For our calculations, we make use of the proxy-SU(3) highest-weight (h.w.) irreps [46,90], to derive a value for the triaxiality parameter [60,61]:

$$\gamma_s = \arctan \left(\frac{\sqrt{3}(\mu+1)}{2\lambda + \mu + 3} \right). \quad (7)$$

We then go on to substitute the above expression, along with Eq. (4), into Eq. (3), obtaining the following IBM-1

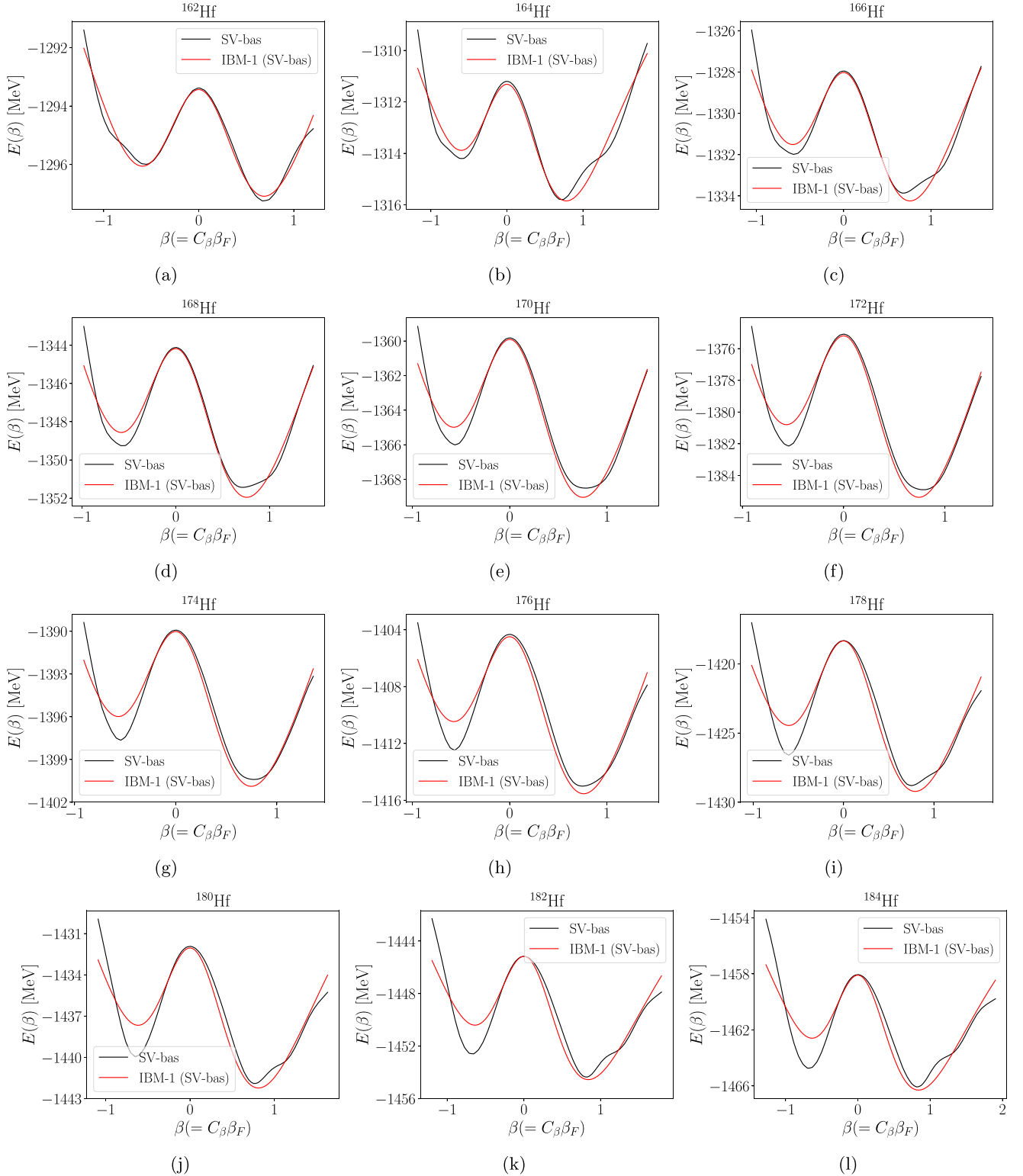
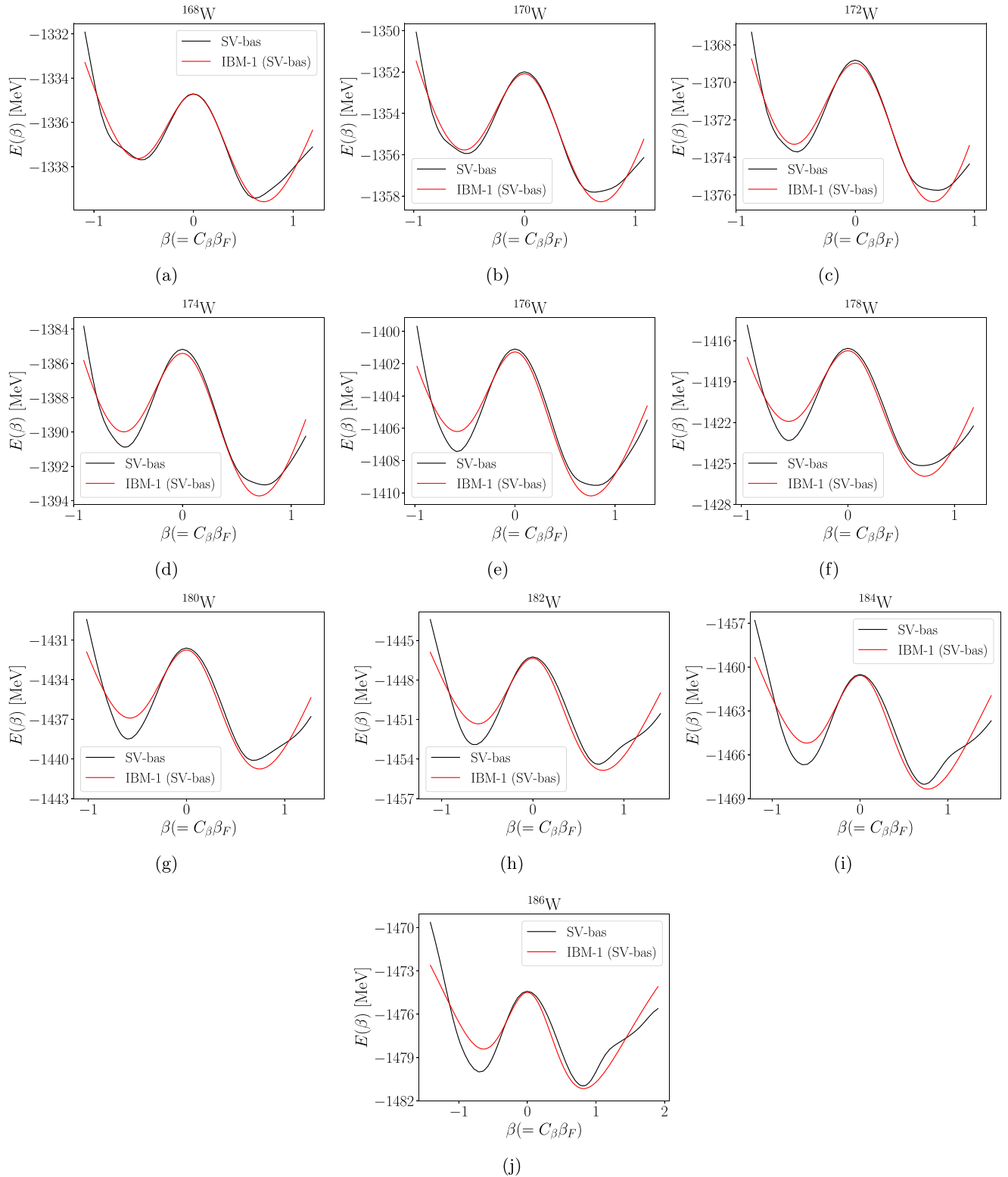


FIG. 1. SV-bas EDF potential energy curves (black) vs the corresponding IBM-1 ones (red), for $^{162-184}\text{Hf}$. The IBM-1 PECs resulted from the mapping process outlined in Sec. II, with the incorporation of proxy-SU(3) irreps.


 FIG. 2. Same as in Fig. 1, for $^{168-186}\text{W}$.

PECs:

$$E(\beta, \gamma = \gamma_s) \rightarrow E(\beta) \equiv E(\beta_F; C_\beta, \chi, \zeta, c, N_B). \quad (8)$$

The same procedure as in the case of $\gamma = 0^\circ$ is then undertaken for the determination of the new values of (χ, ζ, C_β) ,

for each of the studied Hf and W isotopes. The parameters are tabulated in Table II (see also Fig. 7(b) for an indicative level scheme).

In Fig. 2 of the paper [91] the proxy-SU(3) predictions for the deformation variable γ of the Hf and W isotopes under

TABLE I. The parameters of the IBM-1 Hamiltonian of Eq. (1), derived from the mapping process described in Sec. II, for the case of $\gamma = 0^\circ$. The N_B , χ , ζ , c parameters were used as IBAR code inputs for the calculation of energy levels for the ground, β , and γ bands in the studied Hf and W isotopes. Tabulated are also the effective charges, e_B , proportionality coefficients for β deformation, C_β , and the experimental (exp.) and calculated (th.) $R_{4/2}$ energy ratios.

Isotope	N_B	χ	ζ	c [MeV]	e_B [efm ²]	C_β	$R_{4/2}$ (exp.)	$R_{4/2}$ (th.)
¹⁶² Hf	9	-0.185	0.770	2.080	14.7	3.070	2.56	2.58
¹⁶⁴ Hf	10	-0.344	0.820	2.405	16.0	3.070	2.79	2.95
¹⁶⁶ Hf	11	-0.370	0.790	1.956	16.9	2.620	2.97	2.97
¹⁶⁸ Hf	12	-0.357	0.780	1.652	17.0	2.440	3.11	3.00
¹⁷⁰ Hf	13	-0.357	0.760	1.503	16.6	2.260	3.19	3.00
¹⁷² Hf	14	-0.357	0.750	1.473	16.2	2.170	3.25	3.02
¹⁷⁴ Hf	15	-0.370	0.760	1.572	15.2	2.260	3.27	3.11
¹⁷⁶ Hf	16	-0.370	0.770	1.723	14.3	2.350	3.28	3.18
¹⁷⁸ Hf	15	-0.384	0.790	1.790	14.7	2.530	3.29	3.19
¹⁸⁰ Hf	14	-0.384	0.810	1.723	14.7	2.710	3.31	3.19
¹⁸² Hf	13	-0.397	0.830	1.733	14.6	2.980	3.29	3.18
¹⁸⁴ Hf	12	-0.410	0.830	1.725	15.2	3.160	3.26	3.17
¹⁶⁸ W	10	-0.304	0.770	1.870	17.7	2.710	2.82	2.77
¹⁷⁰ W	11	-0.291	0.730	1.423	18.0	2.260	2.95	2.71
¹⁷² W	12	-0.278	0.700	1.084	18.1	1.990	3.06	2.65
¹⁷⁴ W	13	-0.344	0.760	1.549	17.0	2.350	3.15	2.98
¹⁷⁶ W	14	-0.370	0.790	1.871	15.8	2.530	3.22	3.13
¹⁷⁸ W	15	-0.344	0.750	1.713	15.1	2.350	3.24	3.05
¹⁸⁰ W	14	-0.344	0.780	1.689	15.1	2.620	3.26	3.08
¹⁸² W	13	-0.331	0.780	1.448	15.3	2.710	3.29	3.01
¹⁸⁴ W	12	-0.331	0.800	1.529	15.4	2.980	3.27	3.01
¹⁸⁶ W	11	-0.344	0.840	1.685	15.3	3.520	3.23	3.05

study have been compared to the Gogny D1S predictions of Ref. [21], as well as to empirical values, with good agreement seen. This fact adds reliability to the proxy-SU(3) predictions, making them appropriate for use in the present work.

The inclusion of an intrinsic γ deformation, in the form of γ_s , resulting from the use of proxy-SU(3) h.w. irreps has minimal impact on the curvature and overall shape of the

calculated IBM-1 PECs, which are (almost) indistinguishable to the ones obtained in the $\gamma = 0^\circ$ case, with the use of Eq. (6). This is also reflected in the C_β proportionality coefficients tabulated in Tables I and II, which are (nearly) identical in both cases. Thus, only the IBM-1 PECs obtained from Eq. (8) are plotted in Figs. 1(a)–1(i) and 2(a)–2(j), together with the SV-bas EDF PECs, shown for comparison.

As it can be seen from Figs. 3 and 4, the inclusion of an intrinsic γ deformation, through the use of proxy-SU(3)

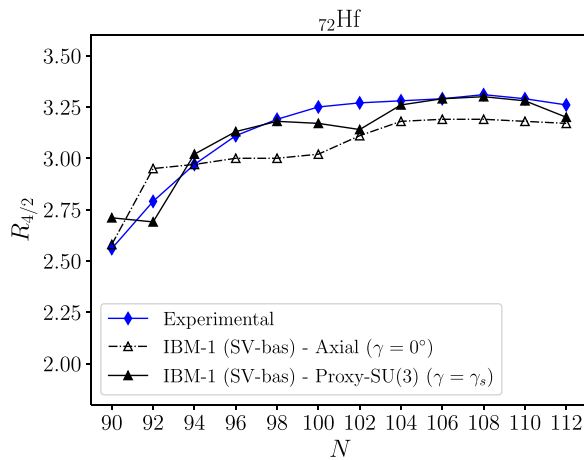


FIG. 3. Experimental (blue diamonds) vs calculated $R_{4/2}$ ratios for ^{162–184}Hf. Results for the case of “pure” axial deformations ($\gamma = 0^\circ$) are shown in empty black triangles, while the predictions made with the use of proxy-SU(3) irreps are plotted in black color with solid symbols (see Sec. II for details on the calculations).

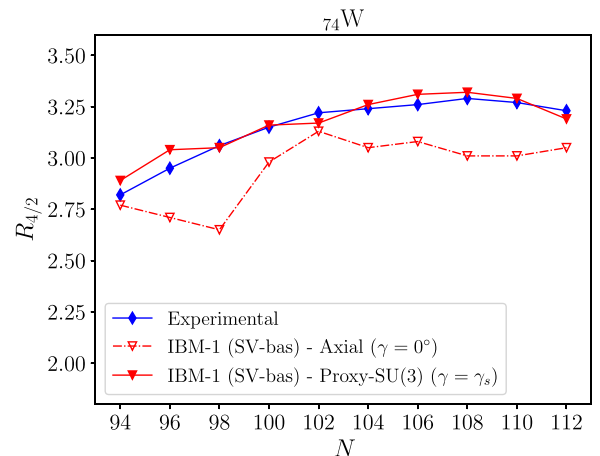


FIG. 4. Same as in Fig. 4, for ^{168–186}W (experimental values shown in blue diamonds, theoretical ones shown in red triangles).

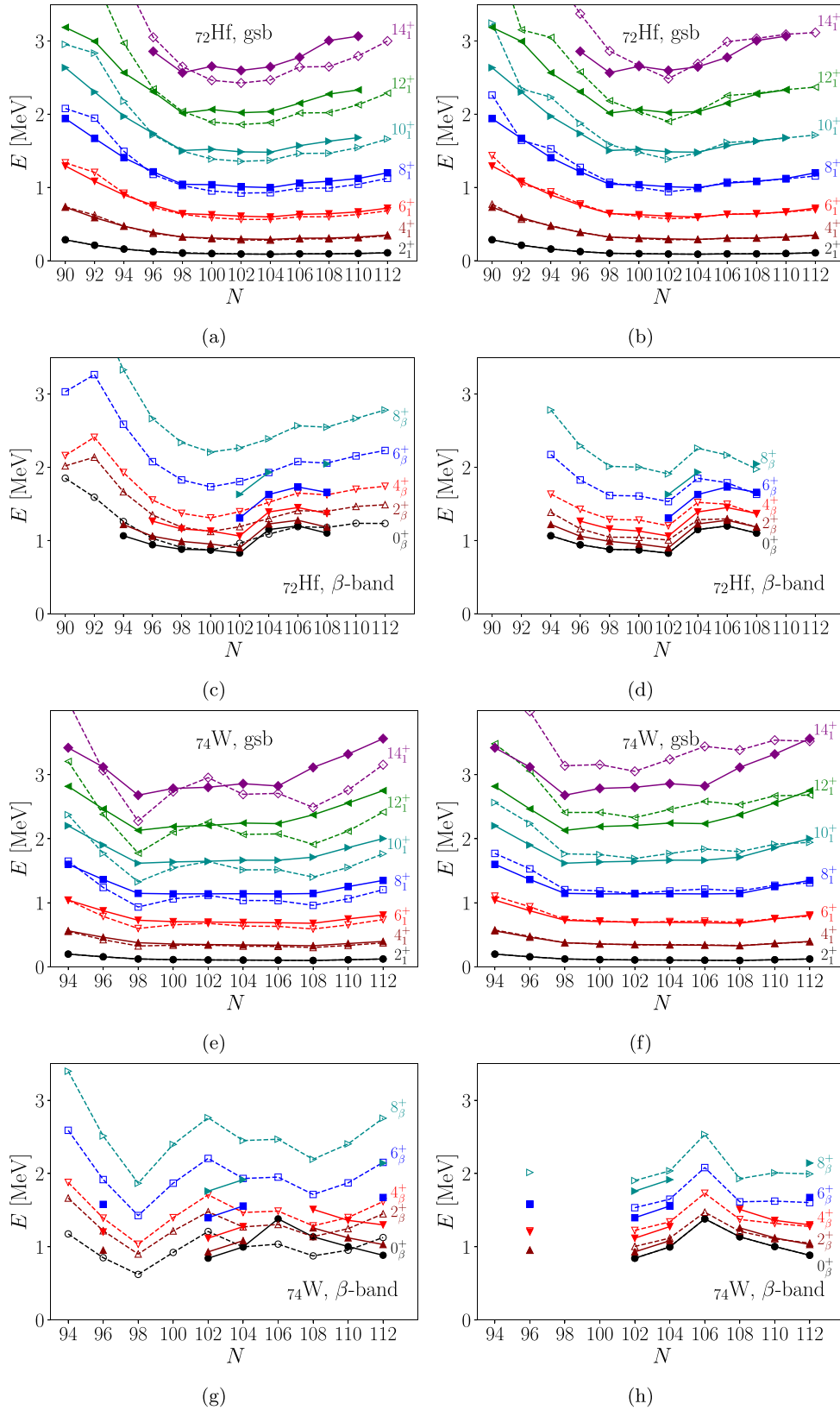


FIG. 5. Experimental (solid lines and symbols) vs theoretical (dashed lines with empty symbols) g.s. and β -band energies for the examined Hf and W isotopes. Calculations with $\gamma = 0^\circ$ are shown in the left column [(a), (c), (e), (g)], while calculations performed with $\gamma = \gamma_s$ and the use of the $\alpha_\beta, \alpha_\gamma$ mass coefficients are shown on the right [(b), (d), (f), (h)].

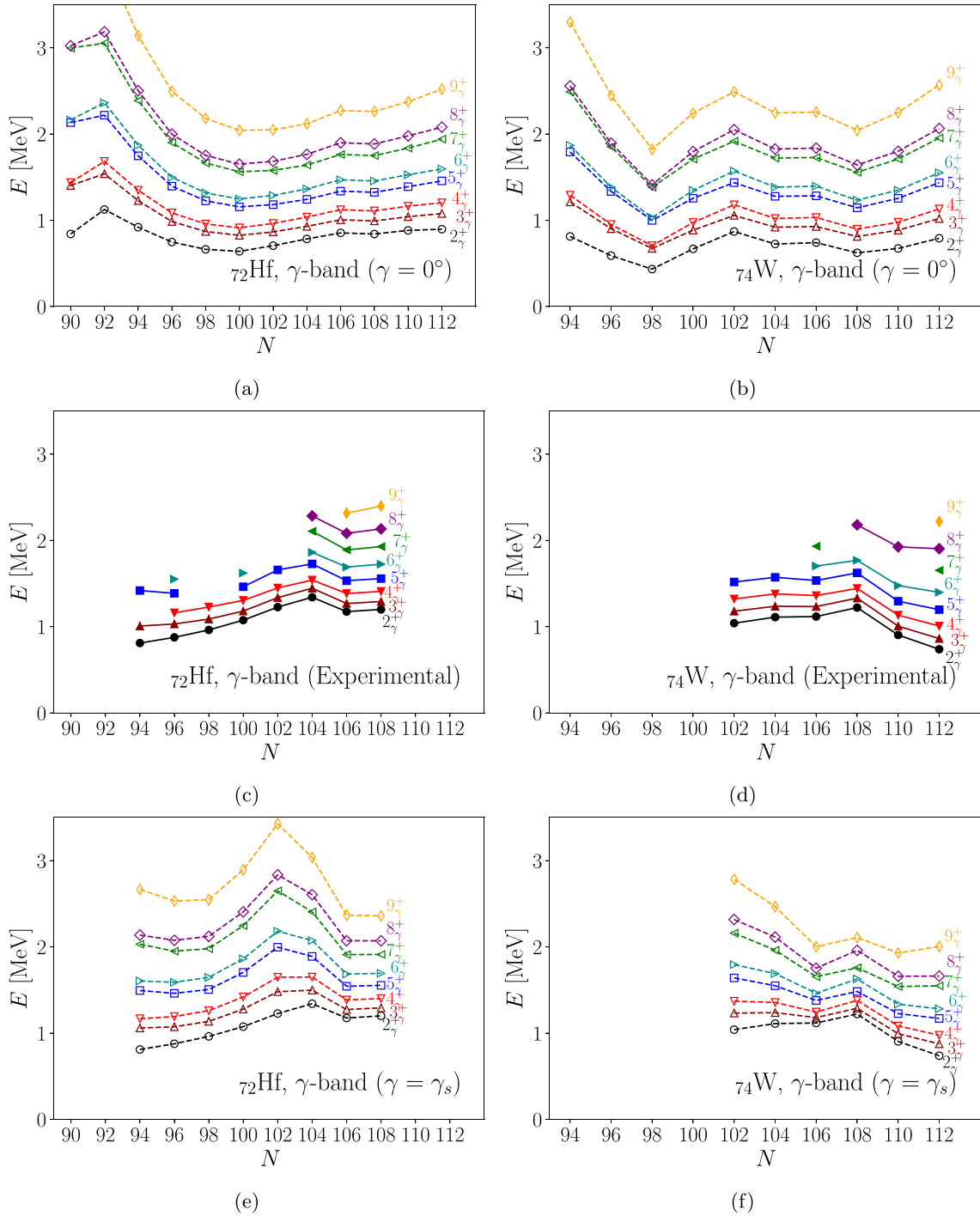


FIG. 6. Similar to Fig. 5, but for the γ bands. Theoretical calculations and experimental data are split into separate panels, to improve readability.

h.w. irreps leads to a significant improvement in the predicted $R_{4/2}$ ratios for the studied isotopes. Additionally, there is a significantly improved agreement for the higher-spin levels of the gsb, which can be attributed to the contribution to the corresponding moment of inertia via the second order Casimir operator of $\text{SU}(3)$ [52–54,92],

$$\hat{C}_2[\text{SU}(3)] = 2\hat{Q} \cdot \hat{Q} + \frac{3}{4}\hat{L}^2, \quad (9)$$

entering implicitly in the calculations via the (λ, μ) irreps used to derive γ_s through Eq. (7). Furthermore, the level spacings for the β bands are much improved, while there is also a vast improvement in the predicted behavior for the staggering inside the γ bands.

For the final step in our calculations, we perform a rescaling of the predicted energy levels for the β and γ bands to the respective experimental band heads, where available (see

TABLE II. The parameters of the IBM-1 Hamiltonian of Eq. (1), derived from the mapping process described in Sec. II, for the case of γ_s . The N_B , χ , ζ , c parameters were used as IBAR code inputs for the calculation of energy levels for the ground, β , and γ bands in the studied Hf and W isotopes. Tabulated are also the effective charges, e_B , proportionality coefficients for β deformation, C_β , the intrinsic γ deformation parameter, γ_s , the experimental (exp.), and calculated (th.) $R_{4/2}$ energy ratios.

Isotope	N_B	χ	ζ	c [MeV]	e_B [efm ²]	C_β	γ_s	$R_{4/2}$ (exp.)	$R_{4/2}$ (th.)
¹⁶² Hf	9	-0.265	0.790	2.370	14.6	3.340	13.923	2.56	2.71
¹⁶⁴ Hf	10	-0.291	0.740	1.759	16.6	3.070	12.834	2.79	2.69
¹⁶⁶ Hf	11	-0.397	0.790	2.015	16.8	2.620	8.308	2.97	3.02
¹⁶⁸ Hf	12	-0.463	0.780	1.841	16.5	2.440	13.407	3.11	3.13
¹⁷⁰ Hf	13	-0.503	0.770	1.672	15.9	2.350	14.840	3.19	3.18
¹⁷² Hf	14	-0.463	0.760	1.638	15.6	2.260	12.949	3.25	3.17
¹⁷⁴ Hf	15	-0.397	0.760	1.616	15.1	2.260	7.735	3.27	3.14
¹⁷⁶ Hf	16	-0.529	0.760	1.893	13.7	2.350	14.840	3.28	3.26
¹⁷⁸ Hf	15	-0.661	0.780	2.066	13.6	2.530	18.793	3.29	3.29
¹⁸⁰ Hf	14	-0.728	0.790	1.998	13.4	2.710	19.423	3.31	3.30
¹⁸² Hf	13	-0.609	0.820	1.925	13.9	2.980	16.558	3.29	3.28
¹⁸⁴ Hf	12	-0.463	0.830	1.796	15.0	3.160	9.339	3.26	3.20
¹⁶⁸ W	10	-0.384	0.770	2.048	17.5	2.710	12.834	2.82	2.89
¹⁷⁰ W	11	-0.503	0.750	1.945	17.0	2.440	18.048	2.95	3.04
¹⁷² W	12	-0.542	0.720	1.600	16.8	2.170	19.423	3.06	3.05
¹⁷⁴ W	13	-0.556	0.740	1.785	16.2	2.260	17.418	3.15	3.16
¹⁷⁶ W	14	-0.450	0.770	1.899	15.6	2.440	11.860	3.22	3.17
¹⁷⁸ W	15	-0.635	0.740	2.122	14.0	2.350	19.423	3.24	3.26
¹⁸⁰ W	14	-0.979	0.740	2.230	12.8	2.530	23.606	3.26	3.31
¹⁸² W	13	-1.111	0.750	2.094	12.4	2.800	24.523	3.29	3.32
¹⁸⁴ W	12	-0.767	0.780	1.994	13.8	2.980	21.772	3.27	3.29
¹⁸⁶ W	11	-0.489	0.830	1.871	14.8	3.520	14.496	3.23	3.19

Table III). This rescaling, which will be discussed in the next section, does not affect the energy ratios or the staggering within individual bands. However, it is necessary in order to obtain quantitative results for the energy levels. The final band levels are presented for the even-even ^{166–180}Hf and ^{170,176–186}W in Figs. 5(b), 5(d), 5(f), 5(h), and 6(e)–6(f) (see also Fig. 7(c) for an indicative level scheme).

Level schemes, similar to those presented for ¹⁸⁰Hf in Fig. 7, are provided for all of the studied Hf and W isotopes in Supplemental Material [93] of this paper.

III. RESULTS AND DISCUSSION

A. Parameter systematics

The parameter systematics tabulated in Tables I and II are plotted in Fig. 8 for the Hf and W isotopes studied in this work. The same notation is used for all of the panels of Fig. 8, i.e., dot-dashed lines with empty symbols for the case of $\gamma = 0^\circ$, solid lines with filled symbols for the case of $\gamma = \gamma_s$, black color for Hf and red for W.

One can immediately notice the relation between the proportionality coefficient, C_β (Fig. 8(a)) and the ζ parameter of the IBM-1 Hamiltonian of Eq. (1) (Fig. 8(b)), related to axial quadrupole deformation. Both parameters follow the same trend, exhibiting minima around the middle of the major shell where the PEC shows the largest deformation. This behavior is in agreement with the results of earlier works of Nomura *et al.* on Xe and Ba isotopes [27], situated in the $N = 50$ –82 major neutron shell, as well as ^{166–194}Hf [49,51], for

the $N = 82$ –126 shell. In the former, an IBM-2 Hamiltonian was mapped to a microscopic PES, derived from Hartree-Fock+BCS calculations employing SLy4 [94] and SkM* [95] effective interactions, while for the latter, a microscopic PES obtained from Hartree-Fock-Bogolyubov calculations with Gogny D1S [96] and D1M [97] EDFs was used for mapping to an IBM-2 Hamiltonian. The C_β values of [49,51] are also plotted in Fig. 8(a), for comparison (green dashed curves with solid squares).

Despite the use of different IBM models (IBM-1 vs IBM-2), pairing schemes (HF+BCS vs HFB), and effective interactions (Skyrme type SV-bas vs Gogny D1M/D1S), there is a very good qualitative agreement between the results presented in this work, and the ones of [49,51], for the Hf isotopes. The quantitative differences for the proportionality coefficients, C_β , can be explained by the use of different effective interactions, leading to larger β_F values for the microscopic PECs/PESs (see e.g. Table VI of [51] for a comparison between Gogny D1M and D1S energy density functionals). Furthermore, depending on the employed EDF, the maximum deformation is observed at either $N = 100$ or 102, 4 or 2 neutrons away from the $N = 104$ midshell, respectively (see also discussion and Fig. 3(a) of [98] for a comparison of quadrupole deformation parameters between various nuclear models). The calculated β_F^{\min} values are plotted as functions of N , together with the experimental data [99], in Figs. 8(c) and 8(d).

It can be seen from Figs. 8(a) and 8(b) that the inclusion of an intrinsic deformation, γ_s , resulting from the use of

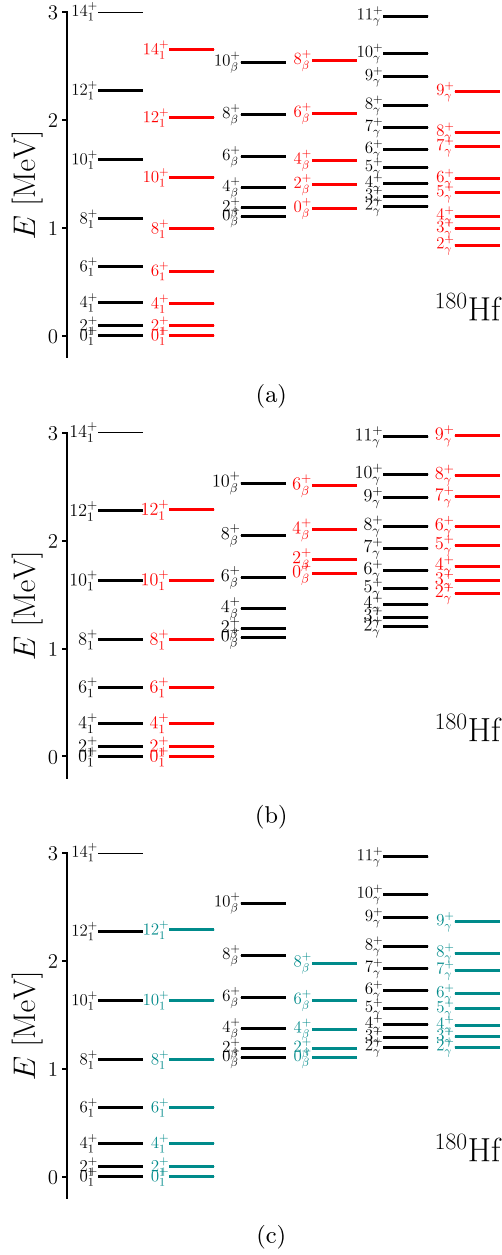


FIG. 7. Experimental (black) vs calculated (red) g.s., β - and γ -band levels of ^{180}Hf , for the case of $\gamma = 0^\circ$ (a) and $\gamma = \gamma_s$ (b). Levels calculated for $\gamma = \gamma_s$, with the use of mass coefficients, are plotted in dark cyan color and compared with the experimental ones (in black) in (c) (see Sec. II for details).

proxy-SU(3) h.w. irreps, has only a minor quantitative effect on C_β , and only in some of the considered Hf and W isotopes.

However, this is not the case for γ_s and χ , the IBM-1 Hamiltonian parameter associated with the degree of triaxiality in the nucleus. As it can be seen from Figs. 8(e) and 8(f), the inclusion of γ_s leads to a drastically different picture for χ , compared to the $\gamma = 0^\circ$ case. Again, the trend of γ_s translates well into χ , with larger values of γ_s leading to larger deformations. These values are more realistic, since they get closer to the SU(3) limit of $\chi = -\sqrt{7}/2 = -1.323$,

TABLE III. Values for the quadrupole deformation parameter at the energy minimum of the HF PECs, denoted as β_F^{\min} , for each of the studied Hf and W isotopes. The mass coefficients for the β (α_β) and γ (α_γ) bands are also tabulated.

Isotope	β_F^{\min}	α_β	α_γ
^{162}Hf	0.208	—	—
^{164}Hf	0.253	—	—
^{166}Hf	0.287	0.803	0.821
^{168}Hf	0.307	0.750	0.893
^{170}Hf	0.317	0.756	1.031
^{172}Hf	0.327	0.799	1.261
^{174}Hf	0.328	0.813	1.616
^{176}Hf	0.328	0.844	1.231
^{178}Hf	0.318	0.716	0.818
^{180}Hf	0.298	0.650	0.795
^{182}Hf	0.278	—	—
^{184}Hf	0.267	—	—
^{168}W	0.262	—	—
^{170}W	0.280	0.578 ^a	0.883
^{172}W	0.296	—	—
^{174}W	0.310	—	—
^{176}W	0.313	0.659	1.058
^{178}W	0.309	0.652	0.819
^{180}W	0.291	0.740	0.553
^{182}W	0.273	0.605	0.576
^{184}W	0.255	0.609	0.585
^{186}W	0.236	0.619	0.673

^aCalculated by replacing 0_β^+ with 2_β^+ in Eq. (12), due to the absence of an experimental value for 0_β^+ in [100].

as is typically the case for well-deformed nuclei. Furthermore, the local minima of γ_s for $N = 102, 112$, which correspond to proxy-SU(3) neutron irreps with $\mu = 0$ [46], are translated into local maxima for χ , in qualitative agreement.

B. Energy spectra

We now proceed to a more thorough examination of the calculated level schemes for the Hf and W isotopes, building upon the first observations made at Sec. II.

Regarding the gsb levels of the studied isotopes, the calculations performed with $\gamma = 0^\circ$ can sufficiently reproduce the energies of the first few low-lying states (up to 8_1^+), with divergences from experimental data making their appearance for higher spins. These divergences have been associated with the moment of inertia, and for well-deformed rotational nuclei, they have been remedied through the inclusion of an additional ($\hat{L} \cdot \hat{L}$) term to the employed IBM Hamiltonian, which provided the experimentally observed $L(L+1)$ level energy dependence [28]. In our calculations, this contribution to the moment of inertia is taken into account implicitly, through the use of h.w. proxy-SU(3) irreps, thus overcoming the need to add extra terms to the IBM-1 ECQF Hamiltonian of Eq. (1).

On the subject of the first $K = 0^+$ excited bands, which are associated with the β bands in this mass region, these are formed by the calculated 0_2^+ , 2_3^+ , 4_3^+ , 6_3^+ , and 8_3^+ states, both in the $\gamma = 0^\circ$ and in the $\gamma = \gamma_s$ cases. However, their

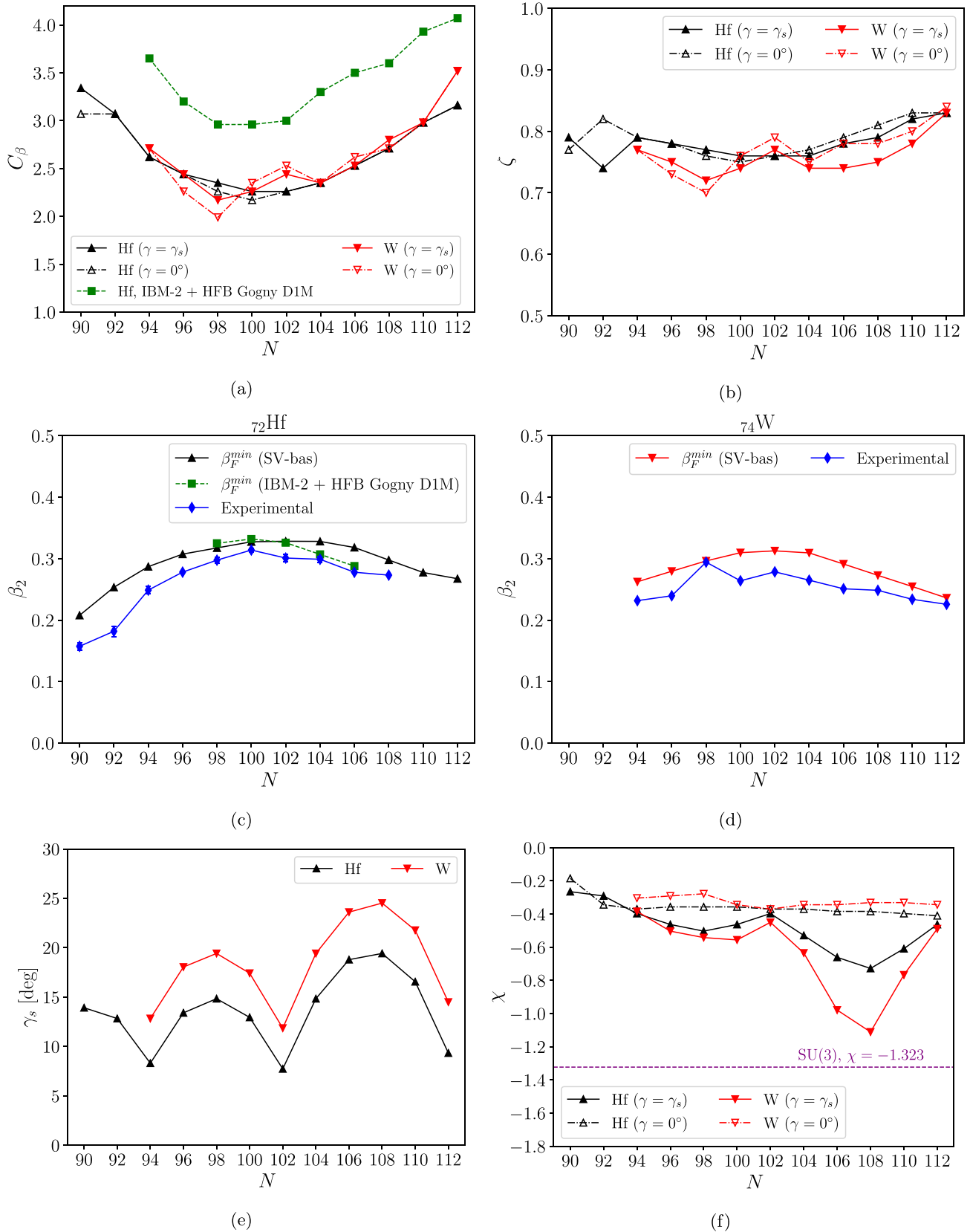


FIG. 8. Systematics for the IBM parameters as functions of the neutron number, N . Experimental quadrupole deformation parameters, β_2 , taken from [99].

structure differs significantly between the two cases, with a behavior assimilating a $\Delta L = 2$ staggering presenting itself for $\gamma = 0^\circ$. Such a behavior has been recently observed also in ^{154}Gd , in the framework of the *sdg*-IBM-1 (see Fig. 3 of [101]), and appears to arise from the assumption of “pure” axial deformations (i.e., axial symmetry at a mean-field level, without any intrinsic triaxial deformation). The inclusion of the intrinsic deformation, γ_s , stemming from the proxy-SU(3) h.w. irreps, is enough to remedy this picture, leading to a good qualitative agreement with the experimental data, while preserving the axial symmetry of the IBM potential energy surface, which is dictated by the $\cos 3\gamma$ term in Eq. (3).

The effect of the proxy-SU(3) irreps is even more impactful on the γ bands, which are formed by the 2_2^+ , 3_1^+ , 4_2^+ , 5_1^+ , ..., 9_1^+ excited states. These bands exhibit a pronounced odd-even staggering, when only axial deformations are assumed (Figs. 6(a), 6(b), and 7(a)). Such a behavior has been observed in the past, in calculations using the mapping method for ^{190}Os , in the framework of *sd*-IBM-2 [102]. The inclusion of a *g* boson ($L = 4$) does not seem to resolve this staggering, which also appeared in ^{154}Gd , in the framework of the *sdg*-IBM-1 [101]. The path followed in [102] to remedy this behavior for the case of ^{190}Os involved the inclusion of a three-body term in the IBM-2 Hamiltonian, of the form

$$H_{3B} = \sum_{\rho \neq \rho'} \theta^\rho [d_\rho^\dagger d_\rho^\dagger d_\rho^\dagger]^{(3)} \cdot [\tilde{d}_{\rho'} \tilde{d}_{\rho'} \tilde{d}_{\rho'}]^{(3)}, \quad \rho = \pi, \nu. \quad (10)$$

The above term is associated with a $\cos^2 3\gamma$ term, capable of producing triaxial minima in the IBM potential energy surface.

In this work, the introduction of the intrinsic triaxial deformation, γ_s , resulting from the proxy-SU(3) h.w. irreps is sufficient to achieve a qualitative agreement with the experimental staggering for the γ bands (Fig. 7(b), see also Supplemental Material [93]), thus avoiding the need for additional terms in the IBM Hamiltonian, and the associated computational complexity arising from the addition of extra parameters.

A final step towards obtaining quantitative results for the energy levels of the β and γ bands in the studied isotopes is undertaken with the inclusion of different mass coefficients for these bands, determined via a rescaling with respect to the experimental band heads, i.e.,

$$E_{\beta(\gamma)}(J) \rightarrow \tilde{E}_{\beta(\gamma)}(J) = \alpha_{\beta(\gamma)} E_\beta(J), \quad (11)$$

where

$$\alpha_\beta = E^{\text{exp.}}(0_\beta^+)/E(0_\beta^+), \quad \alpha_\gamma = E^{\text{exp.}}(2_\gamma^+)/E(2_\gamma^+). \quad (12)$$

The need for the introduction of different mass coefficients in phenomenological models, associated with the varying moments of inertia for different modes of excitation (ground band rotational motion, β and γ vibrations), has been outlined and discussed in the works of Jolos *et al.* (see, e.g., [103–107], and references therein).

However, it should be stressed that the inclusion of different mass coefficients for the β and γ bands does not alter the qualitative picture of the calculations, but rather affects the calculated energy values on a quantitative level. The resulting

band levels are presented for $^{166-180}\text{Hf}$ and $^{170,176-186}\text{W}$ in Figs. 5(b), 5(d), 5(f), 5(h) and Figs. 6(c)–6(f).

Overall, the inclusion of an intrinsic triaxial deformation, resulting from the use of proxy-SU(3) irreps, leads to a significant improvement on the qualitative description of the g.s., β , and γ bands, further improved on the quantitative level with the introduction of different mass coefficients for these bands. The unusually low γ_s predictions of proxy-SU(3), for $N = 94, 102, 112$ (neutron irreps with $\mu = 0$) are also reflected in the IBM-1 calculations. These small γ_s values, while sufficient for the qualitative description of ground state and β bands, are not able to completely remedy the γ -band staggering, leading to a qualitative picture which is closer to the $\gamma = 0^\circ$ case.

C. E2 transitions

We move on to calculate the $B(E2)$ values for some low-lying gsb states. In the ECQF formalism, the relevant transition operator is defined as [29]

$$\hat{T}(E2) = e_B \hat{Q}^\chi, \quad (13)$$

where \hat{Q}^χ is the quadrupole boson creation operator of Eq. (1), and e_B is the effective charge. One option for the determination of the effective charge is the use of a fixed value across the isotopic chain studied, chosen such that it reproduces the experimental $B(E2; 2_1^+ \rightarrow 0_1^+)$ for a specific isotope. However, as shown in previous IBM fitting calculations in the W, Os [108] and Hf [51] isotopic chains, the assumption of a constant value for e_B leads to a maximization of the $B(E2; J \rightarrow J - 2)$ values at the midshell $N = 104$ (^{176}Hf , ^{178}W), in contrast with the experimentally observed maxima at $N = 98$ for W and $N = 100$ for Hf [99].

An alternative for the derivation of the effective charges is the assumption of a mass dependence, with two possible options; the first one is the choice of e_B individually for each nucleus, fitted to the corresponding experimental $B(E2; 2_1^+ \rightarrow 0_1^+)$ values. This is a commonly used approach amongst IBM calculations (see, e.g., [80,81,83,109–111]).

The second one is the choice of e_B individually for each nucleus, such that the intrinsic quadrupole deformation parameter, $\beta_t(2_1^+ \rightarrow 0_1^+)$ of the EDF-IBM model equals the β_F^{min} minimum of the mean-field PEC [51]. More specifically, in the framework of the nuclear collective model, the intrinsic quadrupole deformation parameter, $\beta_t(J \rightarrow J')$ is related to the transition quadrupole moment, $Q_t(J \rightarrow J')$, and the associated $B(E2; J \rightarrow J')$ matrix element, through the relations [12]

$$Q_t(J \rightarrow J') = \sqrt{\frac{16\pi}{5} \frac{B(E2; J \rightarrow J')}{(J200|J'0)^2}} \quad (14)$$

and

$$\beta_t(J \rightarrow J') = \frac{\sqrt{5\pi}}{3ZR^2} Q_t(J \rightarrow J'), \quad (15)$$

where J and J' the spins of the initial and final states, $(J200|J'0)$ the relevant Clebsch-Gordan coefficient, Z the atomic number and R the nuclear radius. By equating $\beta_t(2_1^+ \rightarrow 0_1^+) = \beta_F^{\text{min}}$, one obtains the effective charge, e_B , for each isotope under investigation.

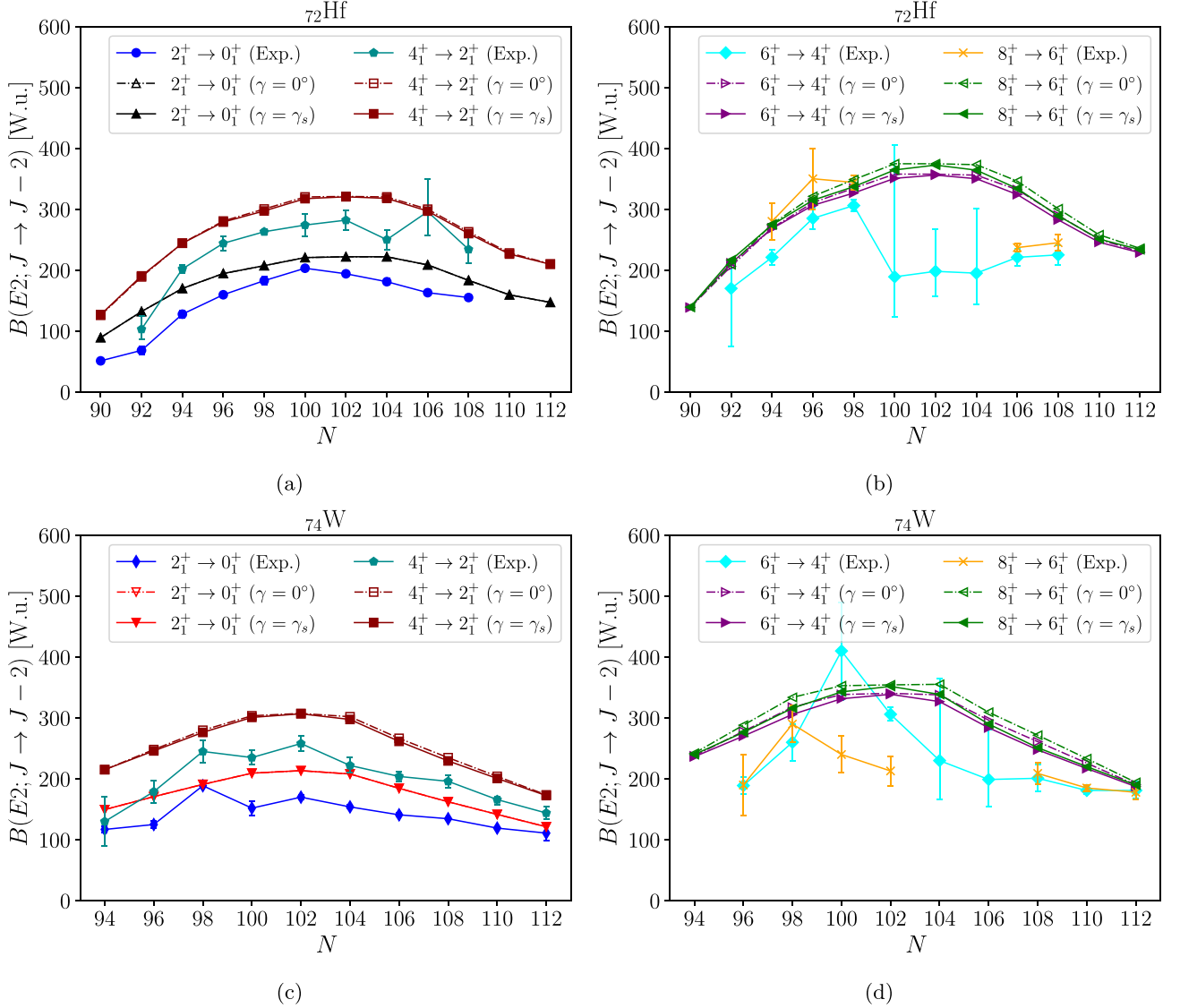


FIG. 9. Experimental vs calculated $B(E2; J \rightarrow J - 2)$ values for the Hf and W isotopes studied in this work. Calculations for $\gamma = 0^\circ$ are shown as dot-dashed lines with open symbols, while solid lines and symbols, of the same color, correspond to calculations for the case of $\gamma = \gamma_s$. Literature data were taken from [99,100,112] for Hf, and [99,100,111] for W.

Since the HF+BCS calculations with the SV-bas EDF give a satisfactory reproduction of the systematics of the β_2 values, and, by extension, the $B(E2; 2_1^+ \rightarrow 0_1^+)$ for the Hf and W isotopic chains, the latter approach is adopted for the derivation of e_B . This choice comes with the advantage of avoiding the addition of extra fitting inputs, albeit at the cost of some small quantitative deviations from the experimental $B(E2)$ values.

For each isotopic chain, two separate sets of e_B are calculated, one for the case of $\gamma = 0^\circ$ and one for $\gamma = \gamma_s$. The resulting $B(E2)$ values are plotted, together with the experimental data existing in the literature [99,100,111,112], in Fig. 9.

A reasonable agreement with the experimental values, on both qualitative and quantitative levels is observed for the $B(E2; 2_1^+ \rightarrow 0_1^+)$ and $B(E2; 4_1^+ \rightarrow 2_1^+)$ transition strengths. This seems to hold true also for $B(E2; 6_1^+ \rightarrow 4_1^+)$ and

$B(E2; 8_1^+ \rightarrow 6_1^+)$, however, the lack of experimental data, and the large uncertainties accompanying the existing ones, prevent a clear comparison between trends for these quantities.

The maximal $B(E2)$ values are obtained for $N = 102$, instead of $N = 100$ for Hf and $N = 98$ for W, which can be attributed to the particular choice of EDF (see also earlier discussion in Sec. III A). This displacement of the maxima with respect to $N = 104$ indicates a saturation of collectivity on the neutron-deficient side, as one moves towards the neutron midshell in the examined isotopic chains. The pre-midshell saturation of the $B(E2)$ transition strengths, which gets more pronounced with increasing proton numbers, was partially attributed in [113] to the influence of a hexadecapole deformation, β_4 , entering the expression for the transitional quadrupole moment, Q_t . In the sd -IBM framework, such an effect, caused by the renormalization of g bosons, could be

incorporated to an extent via an expansion of the expression for the quadrupole operator of Eq. (1), made to include higher-order (two-body) terms [51,113]. A more extensive study on the influence of hexadecapole deformations on $B(E2; 2_1^+ \rightarrow 0_1^+)$ was undertaken for the even-even nuclei of the Er-Yb-Hf-W mass region in [112], however, it could not offer a complete explanation of the early $B(E2)$ maxima.

The $B(E2)$ systematics calculated in this work are consistent with earlier findings of Ref. [51,112] on $^{166-180}\text{Hf}$ and Ref. [111,112] on $^{172-182}\text{W}$, while at the same time expanding the area of study towards the more neutron deficient side of these isotopic chains.

It should be noted that the inclusion of an intrinsic triaxial deformation, γ_s , generated through the proxy-SU(3) irreps, has minimal influence on the $B(E2)$ values for the gsb transitions examined. More specifically, it leads to a lowering of the $B(E2)$ predictions, which gets slightly more pronounced for higher-spin states (Fig. 9). Overall, the $B(E2)$ strengths appear to exhibit similar sensitivity to the inclusion of γ_s compared to C_β , which is not unexpected, given their connection to the quadrupole deformation parameters [see also Eqs. (14) and (15)].

IV. SUMMARY AND OUTLOOK

In view of recent findings, which indicate the presence of some degree of triaxiality all over the nuclear chart [35–37], an effort is made to include triaxiality in the framework of the standard IBM-1, in which only one- and two-body terms are taken into account, and no distinction between protons and neutrons is made. The aim of this effort is to provide an easy tool (the existing IBM code [29]) for calculating spectra and $B(E2)$ transition rates for many medium-mass and heavy nuclei.

Along the path taken, potential energy curves are calculated using a self-consistent mean-field approach employing a Skyrme energy density functional, namely the axial Hartree-Fock+BCS code SKYAX [48]. The PECs derived by IBM-1 are then fitted to the microscopic PECs, in order to have the IBM-1 parameters determined. Once this is done, spectra and $B(E2)$ transition rates for the nuclei under study are readily obtained through the IBAR code [29].

Two sets of calculations have been performed, one assuming axial symmetry, as it is the case in the original IBM-1 with only one- and two-body terms included in the Hamiltonian, and an additional one, in which an intrinsic triaxial deformation has been added to the potential energy curve corresponding to the classical limit of IBM-1. The intrinsic triaxial deformation has not been treated as a free parameter; on the contrary, it has been obtained from the proxy-SU(3) approximation to the shell model [45–47] in a parameter-free

way, taking into account the Pauli principle and the short-range nature of the nucleon-nucleon interaction.

Significantly improved results have been obtained in the latter case, providing an *a posteriori* justification for the inclusion of a microscopically derived intrinsic triaxial deformation in the potential energy curve corresponding to the classical limit of IBM-1.

In conclusion, the preponderance of triaxial shapes over most of the nuclear chart is predicted in a parameter-free way by the proxy-SU(3) approximation to the shell model, while detailed predictions for spectra and $B(E2)$ transition rates for specific nuclei can be readily calculated through the IBM-1 code IBAR [29] after including an intrinsic triaxial deformation to the potential energy curve of the IBM-1 in its classical limit, and determining the IBM-1 parameters through fitting of the resulting potential energy curve to the one derived through the axial Hartree-Fock+BCS code SKYAX [48].

In the present work, the Hf and W series of isotopes have been used as the test ground of the new approach. A region of obvious interest for further calculations consists of the Os and Pt series of isotopes, for which sufficient experimental data exist for chains of isotopes ranging from moderate to strong quadrupole deformation, extending beyond $N = 116$, where a prolate to oblate shape/phase transition is expected to take place [46,114–117].

It would be interesting to examine if and how much the results of the present approach would be influenced by fitting the IBM-1 PEC with intrinsic triaxial deformation to a microscopic PEC derived by a self-consistent mean-field approach including triaxiality [118,119]. Recent calculations in the Ce isotopes [120] have indicated that triaxiality appears only for $N < 82$, but the validity of this result has to be checked at higher Z .

Regarding the Hf and W isotopes studied in the present work, triaxial mean-field calculations performed in the framework of the HFB formalism with the Gogny D1S EDF [21] result in axially symmetric PESSs, with minima along the $\gamma = 0^\circ$ line of the β - γ plane. These calculations are available in the AMEDEF database [121] (see column 5 in the table of [122]). The γ deformation at the HFB energy minimum is 0° for all of the examined Hf and W isotopes (with the exception of ^{180}W , for which $\gamma = 1^\circ \simeq 0^\circ$). This is consistent with the results of similar calculations found in Refs. [49,51], which were carried out on the β - γ plane with the HFB + Gogny D1S and D1M EDFs, and the results of the present work.

Still, many of the constrained mean-field calculations performed with triaxial quadrupole deformations give energy surfaces that have a triaxial minimum or are considerably γ soft. This might play a role as one moves on to examine more axially asymmetric nuclei (e.g., Os and Pt), making for an interesting future study subject.

[1] M. G. Mayer and J. H. D. Jensen, *Elementary Theory of Nuclear Shell Structure* (Wiley, New York, 1955).

[2] K. L. G. Heyde, *The Nuclear Shell Model* (Springer, Berlin, 1990).

[3] I. Talmi, *Simple Models of Complex Nuclei: The Shell Model and the Interacting Boson Model* (Harwood, Chur, 1993).

[4] B. G. Wybourne, *Classical Groups for Physicists* (Wiley, New York, 1974).

- [5] M. Moshinsky and Y. F. Smirnov, *The Harmonic Oscillator in Modern Physics* (Harwood, Amsterdam, 1996).
- [6] F. Iachello, *Lie Algebras and Applications* (Springer, Berlin, 2006).
- [7] P. Navrátil, J. P. Vary, and B. R. Barrett, Large-basis *ab initio* no-core shell model and its application to ^{12}C , *Phys. Rev. C* **62**, 054311 (2000).
- [8] T. Dytrych, K. D. Sviratcheva, J. P. Draayer, C. Bahri, and J. P. Vary, *Ab initio* symplectic no-core shell model, *J. Phys. G: Nucl. Part. Phys.* **35**, 123101 (2008).
- [9] K. D. Launey, T. Dytrych, G. H. Sargsyan, R. B. Baker, and J. P. Draayer, Emergent symplectic symmetry in atomic nuclei: *Ab initio* symmetry-adapted no-core shell model, *Eur. Phys. J.: Spec. Top.* **229**, 2429 (2020).
- [10] A. Bohr, The coupling of nuclear surface oscillations to the motion of individual nucleons, *Mat. Fys. Medd. K. Dan. Vidensk. Selsk.* **26**, 14 (1952).
- [11] A. Bohr and B. R. Mottelson, *Nuclear Structure*, Vol. I: Single-Particle Motion (World Scientific Publishing, Singapore, 1998).
- [12] A. Bohr and B. R. Mottelson, *Nuclear Structure*, Vol. II: Nuclear Deformations (World Scientific Publishing, Singapore, 1998).
- [13] F. Iachello and A. Arima, *The Interacting Boson Model*, Cambridge Monographs on Mathematical Physics (Cambridge University Press, Cambridge, 1987).
- [14] A. Arima and F. Iachello, Interacting boson model of collective states I. The vibrational limit, *Ann. Phys.* **99**, 253 (1976).
- [15] A. Arima and F. Iachello, Interacting boson model of collective nuclear states II. The rotational limit, *Ann. Phys.* **111**, 201 (1978).
- [16] A. Arima and F. Iachello, Interacting boson model of collective nuclear states IV. The $O(6)$ limit, *Ann. Phys.* **123**, 468 (1979).
- [17] J. N. Ginocchio and M. W. Kirson, Relationship between the bohr collective Hamiltonian and the interacting-boson model, *Phys. Rev. Lett.* **44**, 1744 (1980).
- [18] J. Ginocchio and M. Kirson, An intrinsic state for the interacting boson model and its relationship to the Bohr-Mottelson model, *Nucl. Phys. A* **350**, 31 (1980).
- [19] A. E. L. Dieperink, O. Scholten, and F. Iachello, Classical limit of the interacting-boson model, *Phys. Rev. Lett.* **44**, 1747 (1980).
- [20] M. Bender, P.-H. Heenen, and P.-G. Reinhard, Self-consistent mean-field models for nuclear structure, *Rev. Mod. Phys.* **75**, 121 (2003).
- [21] J. P. Delaroche, M. Girod, J. Libert, H. Goutte, S. Hilaire, S. Péru, N. Pillet, and G. F. Bertsch, Structure of even-even nuclei using a mapped collective Hamiltonian and the D1S Gogny interaction, *Phys. Rev. C* **81**, 014303 (2010).
- [22] J. Erler, P. Klüpfel, and P. G. Reinhard, Self-consistent nuclear mean-field models: Example Skyrme-Hartree-Fock, *J. Phys. G: Nucl. Part. Phys.* **38**, 033101 (2011).
- [23] G. A. Lalazissis, J. König, and P. Ring, New parametrization for the Lagrangian density of relativistic mean field theory, *Phys. Rev. C* **55**, 540 (1997).
- [24] D. Vretenar, A. V. Afanasjev, G. A. Lalazissis, and P. Ring, Relativistic Hartree-Bogoliubov theory: Static and dynamic aspects of exotic nuclear structure, *Phys. Rep.* **409**, 101 (2005).
- [25] T. Nikšić, N. Paar, D. Vretenar, and P. Ring, DIRHB—A relativistic self-consistent mean-field framework for atomic nuclei, *Comput. Phys. Commun.* **185**, 1808 (2014).
- [26] K. Nomura, N. Shimizu, and T. Otsuka, Mean-field derivation of the interacting boson model Hamiltonian and exotic nuclei, *Phys. Rev. Lett.* **101**, 142501 (2008).
- [27] K. Nomura, N. Shimizu, and T. Otsuka, Formulating the interacting boson model by mean-field methods, *Phys. Rev. C* **81**, 044307 (2010).
- [28] K. Nomura, T. Otsuka, N. Shimizu, and L. Guo, Microscopic formulation of the interacting boson model for rotational nuclei, *Phys. Rev. C* **83**, 041302(R) (2011).
- [29] R. Casperson, IBAR: Interacting boson model calculations for large system sizes, *Comput. Phys. Commun.* **183**, 1029 (2012).
- [30] A. S. Davydov and G. F. Filippov, Rotational states in even atomic nuclei, *Nucl. Phys.* **8**, 237 (1958).
- [31] A. S. Davydov and V. S. Rostovsky, Relative transition probabilities between rotational levels of non-axial nuclei, *Nucl. Phys.* **12**, 58 (1959).
- [32] J. Meyer-Ter-Vehn, Collective model description of transitional odd-A nuclei: (I). The triaxial-rotor-plus-particle model, *Nucl. Phys. A* **249**, 111 (1975).
- [33] N. V. Zamfir and R. F. Casten, Signatures of γ softness or triaxiality in low energy nuclear spectra, *Phys. Lett. B* **260**, 265 (1991).
- [34] E. A. McCutchan, D. Bonatsos, N. V. Zamfir, and R. F. Casten, Staggering in γ -band energies and the transition between different structural symmetries in nuclei, *Phys. Rev. C* **76**, 024306 (2007).
- [35] Y. Tsunoda and T. Otsuka, Triaxial rigidity of ^{166}Er and its Bohr-model realization, *Phys. Rev. C* **103**, L021303 (2021).
- [36] T. Otsuka, Y. Tsunoda, Y. Utsuno, N. Shimizu, T. Abe, and H. Ueno, Prevailing triaxial shapes in heavy nuclei driven by nuclear tensor force, [arXiv:2303.11299](https://arxiv.org/abs/2303.11299).
- [37] S. Rouoof, N. Nazir, S. Jehangir, G. H. Bhat, J. A. Sheikh, N. Rather, and S. Frauendorf, Fingerprints of the triaxial deformation from energies and $B(E2)$ transition probabilities of γ -bands in transitional and deformed nuclei, *Eur. Phys. J. A* **60**, 40 (2024).
- [38] P. Van Isacker and J.-Q. Chen, Classical limit of the interacting boson Hamiltonian, *Phys. Rev. C* **24**, 684 (1981).
- [39] K. Heyde, P. Van Isacker, M. Waroquier, and J. Moreau, Triaxial shapes in the interacting boson model, *Phys. Rev. C* **29**, 1420 (1984).
- [40] G. Thiamova, The IBM description of triaxial nuclei, *Eur. Phys. J. A* **45**, 81 (2010).
- [41] L. Fortunato, C. E. Alonso, J. M. Arias, J. E. García-Ramos, and A. Vitturi, Phase diagram for a cubic- Q interacting boson model Hamiltonian: Signs of triaxiality, *Phys. Rev. C* **84**, 014326 (2011).
- [42] A. E. L. Dieperink and R. Bijker, On triaxial features in the neutron-proton IBA, *Phys. Lett. B* **116**, 77 (1982).
- [43] N. R. Walet and P. J. Brussaard, A study of the $SU(3)^*$ limit of IBM-2, *Nucl. Phys. A* **474**, 61 (1987).
- [44] A. Sevrin, K. Heyde, and J. Jolie, Triaxiality in the proton-neutron interacting boson model: Systematic study of perturbations in the $SU^{/emph>(3)}$ limit, *Phys. Rev. C* **36**, 2621 (1987).

- [45] D. Bonatsos, I. E. Assimakis, N. Minkov, A. Martinou, R. B. Cakirli, R. F. Casten, and K. Blaum, Proxy-SU(3) symmetry in heavy deformed nuclei, *Phys. Rev. C* **95**, 064325 (2017).
- [46] D. Bonatsos, I. E. Assimakis, N. Minkov, A. Martinou, S. Sarantopoulou, R. B. Cakirli, R. F. Casten, and K. Blaum, Analytic predictions for nuclear shapes, prolate dominance, and the prolate-oblate shape transition in the proxy-SU(3) model, *Phys. Rev. C* **95**, 064326 (2017).
- [47] D. Bonatsos, A. Martinou, S. K. Peroulis, T. J. Mertzimekis, and N. Minkov, The proxy-SU(3) symmetry in atomic nuclei, *Symmetry* **15**, 169 (2023).
- [48] P.-G. Reinhard, B. Schuetrumpf, and J. Maruhn, The axial Hartree-Fock + BCS code SKYAX, *Comput. Phys. Commun.* **258**, 107603 (2021).
- [49] K. Nomura, T. Otsuka, R. Rodríguez-Guzmán, L. M. Robledo, and P. Sarriguren, Collective structural evolution in neutron-rich Yb, Hf, W, Os, and Pt isotopes, *Phys. Rev. C* **84**, 054316 (2011).
- [50] K. Nomura, T. Otsuka, R. Rodríguez-Guzmán, L. M. Robledo, P. Sarriguren, P. H. Regan, P. D. Stevenson, and Z. Podolyák, Spectroscopic calculations of the low-lying structure in exotic Os and W isotopes, *Phys. Rev. C* **83**, 054303 (2011).
- [51] M. Rudigier, K. Nomura, M. Dannhoff, R.-B. Gerst, J. Jolie, N. Saed-Samii, S. Stegemann, J.-M. Régis, L. M. Robledo, R. Rodríguez-Guzmán, A. Blazhev, C. Fransen, N. Warr, and K. O. Zell, Evolution of $E2$ transition strength in deformed hafnium isotopes from new measurements on ^{172}Hf , ^{174}Hf , and ^{176}Hf , *Phys. Rev. C* **91**, 044301 (2015).
- [52] J. P. Elliott, Collective motion in the nuclear shell model. I. Classification schemes for states of mixed configurations, *Proc. R. Soc. London A* **245**, 128 (1958).
- [53] J. P. Elliott, Collective motion in the nuclear shell model II. The introduction of intrinsic wave-functions, *Proc. R. Soc. London A* **245**, 562 (1958).
- [54] J. P. Elliott and M. Harvey, Collective motion in the nuclear shell model III. The calculation of spectra, *Proc. R. Soc. London A* **272**, 557 (1963).
- [55] A. Martinou, D. Bonatsos, N. Minkov, I. E. Assimakis, S. K. Peroulis, S. Sarantopoulou, and J. Cseh, Proxy-SU(3) symmetry in the shell model basis, *Eur. Phys. J. A* **56**, 239 (2020).
- [56] D. Bonatsos, H. Sobhani, and H. Hassanabadi, Shell model structure of proxy-SU(3) pairs of orbitals, *Eur. Phys. J. Plus* **135**, 710 (2020).
- [57] S. G. Nilson, Binding states of individual nucleons in strongly deformed nuclei, *Mat. Fys. Medd. K. Dan. Vidensk. Selsk.* **29**, 1 (1955).
- [58] S. G. Nilson and I. Ragnarsson, *Shapes and Shells in Nuclear Structure* (Cambridge University Press, Cambridge, 1995).
- [59] A. Martinou, D. Bonatsos, K. E. Karakatsanis, S. Sarantopoulou, I. E. Assimakis, S. K. Peroulis, and N. Minkov, Why nuclear forces favor the highest weight irreducible representations of the fermionic SU(3) symmetry, *Eur. Phys. J. A* **57**, 83 (2021).
- [60] O. Castaños, J. P. Draayer, and Y. Leschber, Shape variables and the shell model, *Z. Phys. A* **329**, 33 (1988).
- [61] J. P. Draayer, S. C. Park, and O. Castaños, Shell-model interpretation of the collective-model potential-energy surface, *Phys. Rev. Lett.* **62**, 20 (1989).
- [62] I. Hamamoto and B. R. Mottelson, Further examination of prolate-shape dominance in nuclear deformation, *Phys. Rev. C* **79**, 034317 (2009).
- [63] I. Hamamoto and B. Mottelson, Shape deformations in atomic nuclei, *Scholarpedia* **7**, 10693 (2012).
- [64] ENSDF, <https://www.nndc.bnl.gov/ensdf>.
- [65] R. F. Casten, *Nuclear Structure from a Simple Perspective* (Oxford University Press, Oxford, 2000).
- [66] L. Esser, U. Neuneyer, R. F. Casten, and P. von Brentano, Correlations of the deformation variables β and γ in even-even Hf, W, Os, Pt, and Hg nuclei, *Phys. Rev. C* **55**, 206 (1997).
- [67] R. F. Casten and D. D. Warner, The interacting boson approximation, *Rev. Mod. Phys.* **60**, 389 (1988).
- [68] R. D. Ratna Raju, J. P. Draayer, and K. T. Hecht, Search for a coupling scheme in heavy deformed nuclei: The pseudo SU(3) model, *Nucl. Phys. A* **202**, 433 (1973).
- [69] J. P. Draayer, K. J. Weeks, and K. T. Hecht, Strength of the $Q_\pi \cdot Q_\nu$ interaction and the strong-coupled pseudo-SU(3) limit, *Nucl. Phys. A* **381**, 1 (1982).
- [70] J. P. Draayer and K. J. Weeks, Towards a shell model description of the low-energy structure of deformed nuclei I. Even-even systems, *Ann. Phys.* **156**, 41 (1984).
- [71] P. Klüpfel, P.-G. Reinhard, T. J. Bürvenich, and J. A. Maruhn, Variations on a theme by Skyrme: A systematic study of adjustments of model parameters, *Phys. Rev. C* **79**, 034310 (2009).
- [72] M. Abolghasem and P. Alexa, Microscopic study of ground-state binding energies in $Z = 52-70$ neutron-rich nuclei, *Nucl. Phys. A* **1044**, 122841 (2024).
- [73] P. Lipas, P. Toivonen, and D. Warner, IBA consistent-Q formalism extended to the vibrational region, *Phys. Lett. B* **155**, 295 (1985).
- [74] D. D. Warner and R. F. Casten, Revised formulation of the phenomenological interacting boson approximation, *Phys. Rev. Lett.* **48**, 1385 (1982).
- [75] D. D. Warner and R. F. Casten, Predictions of the interacting boson approximation in a consistent Q framework, *Phys. Rev. C* **28**, 1798 (1983).
- [76] N. V. Zamfir, P. von Brentano, R. F. Casten, and J. Jolie, Test of two-level crossing at the $N = 90$ spherical-deformed critical point, *Phys. Rev. C* **66**, 021304(R) (2002).
- [77] V. Werner, P. von Brentano, R. Casten, C. Scholl, E. McCutchan, R. Krücken, and J. Jolie, Alternative interpretation of $E0$ strengths in transitional regions, *Eur. Phys. J. A* **25**, 455 (2005).
- [78] D. H. Feng, R. Gilmore, and S. R. Deans, Phase transitions and the geometric properties of the interacting boson model, *Phys. Rev. C* **23**, 1254 (1981).
- [79] F. Iachello, N. V. Zamfir, and R. F. Casten, Phase coexistence in transitional nuclei and the interacting-boson model, *Phys. Rev. Lett.* **81**, 1191 (1998).
- [80] E. A. McCutchan, N. V. Zamfir, and R. F. Casten, Mapping the interacting boson approximation symmetry triangle: New trajectories of structural evolution of rare-earth nuclei, *Phys. Rev. C* **69**, 064306 (2004).
- [81] A. Zyriliou, T. J. Mertzimekis, A. Chalil, P. Vasileiou, E. Mavrommatis, D. Bonatsos, A. Martinou, S. Peroulis, and N. Minkov, A study of some aspects of the nuclear structure in the even-even Yb isotopes, *Eur. Phys. J. Plus* **137**, 352 (2022).
- [82] F. Iachello and A. Arima, *The Interacting Boson Model*, Cambridge Monographs on Mathematical Physics (Cambridge University Press, Cambridge, 1987).

- [83] E. A. McCutchan, D. Bonatsos, and N. V. Zamfir, Connecting the $X(5)-\beta^2$, $X(5)-\beta^4$, and $X(3)$ models to the shape/phase-transition region of the interacting boson model, *Phys. Rev. C* **74**, 034306 (2006).
- [84] R. F. Casten, A. Aprahamian, and D. D. Warner, Axial asymmetry and the determination of effective γ values in the interacting boson approximation, *Phys. Rev. C* **29**, 356 (1984).
- [85] Y. Zhang, F. Pan, L.-R. Dai, and J. P. Draayer, Triaxial rotor in the $SU(3)$ limit of the interacting boson model, *Phys. Rev. C* **90**, 044310 (2014).
- [86] Y. Zhang, Y.-W. He, D. Karlsson, C. Qi, F. Pan, and J. Draayer, A theoretical interpretation of the anomalous reduced $E2$ transition probabilities along the yrast line of neutron-deficient nuclei, *Phys. Lett. B* **834**, 137443 (2022).
- [87] Y. Leschber and J. Draayer, Algebraic realization of rotational dynamics, *Phys. Lett. B* **190**, 1 (1987).
- [88] C. Naqvi, H. A. Bahri, D. Troltenier, J. P. Draayer, and A. Faessler, Algebraic realization of the quantum rotor-odd- A nuclei, *Z. Phys. A* **351**, 259 (1995).
- [89] Y. F. Smirnov, N. A. Smirnova, and P. Van Isacker, $SU(3)$ realization of the rigid asymmetric rotor within the interacting boson model, *Phys. Rev. C* **61**, 041302(R) (2000).
- [90] A. Martinou, D. Bonatsos, T. J. Mertzimekis, K. E. Karakatsanis, I. E. Assimakis, S. K. Peroulis, S. Sarantopoulou, and N. Minkov, The islands of shape coexistence within the Elliott and the proxy- $SU(3)$ models, *Eur. Phys. J. A* **57**, 84 (2021).
- [91] A. Martinou, D. Bonatsos, I. E. Assimakis, N. Minkov, S. Sarantopoulou, R. B. Cakirli, R. F. Casten, and K. Blaum, Parameter free predictions within the proxy- $SU(3)$ model, *Bulg. J. Phys.* **44**, 407 (2017).
- [92] J. P. Elliott and C. E. Wilsdon, Collective motion in the nuclear shell model IV. Odd-mass nuclei in the sd shell, *Proc. R. Soc. London A* **302**, 509 (1968).
- [93] See Supplemental Material at <http://link.aps.org/supplemental/10.1103/PhysRevC.110.014313> for level schemes of $^{162-184}\text{Hf}$ and $^{168-186}\text{W}$.
- [94] E. Chabanat, P. Bonche, P. Haensel, J. Meyer, and R. Schaeffer, A Skyrme parametrization from subnuclear to neutron star densities Part II. Nuclei far from stabilities, *Nucl. Phys. A* **635**, 231 (1998).
- [95] J. Bartel, P. Quentin, M. Brack, C. Guet, and H.-B. Håkansson, Towards a better parametrisation of Skyrme-like effective forces: A critical study of the SkM force, *Nucl. Phys. A* **386**, 79 (1982).
- [96] J. Berger, M. Girod, and D. Gogny, Microscopic analysis of collective dynamics in low energy fission, *Nucl. Phys. A* **428**, 23 (1984).
- [97] S. Goriely, S. Hilaire, M. Girod, and S. Péru, First Gogny-Hartree-Fock-Bogoliubov nuclear mass model, *Phys. Rev. Lett.* **102**, 242501 (2009).
- [98] P. Vasileiou, T. J. Mertzimekis, E. Mavrommatis, and A. Zyriliou, Nuclear structure investigations of even-even Hf isotopes, *Symmetry* **15**, 196 (2023).
- [99] B. Pritychenko, M. Birch, B. Singh, and M. Horoi, Tables of $E2$ transition probabilities from the first 2^+ states in even-even nuclei, *At. Data Nucl. Data Tables* **107**, 1 (2016).
- [100] National Nuclear Data Center, <https://www.nndc.bnl.gov/nudat3>.
- [101] L. Lotina and K. Nomura, Impacts of hexadecapole deformations on the collective energy spectra of axially deformed nuclei, *Phys. Rev. C* **109**, 034304 (2024).
- [102] K. Nomura, N. Shimizu, D. Vretenar, T. Nikšić, and T. Otsuka, Robust regularity in γ -soft nuclei and its microscopic realization, *Phys. Rev. Lett.* **108**, 132501 (2012).
- [103] R. V. Jolos, P. von Brentano, and N. Pietralla, Generalized Grodzins relation, *Phys. Rev. C* **71**, 044305 (2005).
- [104] R. V. Jolos, P. von Brentano, A. Dewald, and N. Pietralla, Spin dependence of intrinsic and transition quadrupole moments, *Phys. Rev. C* **72**, 024310 (2005).
- [105] R. V. Jolos and P. von Brentano, Mass coefficient and Grodzins relation for the ground-state band and γ band, *Phys. Rev. C* **74**, 064307 (2006).
- [106] R. V. Jolos and P. von Brentano, Bohr Hamiltonian with different mass coefficients for the ground and γ bands from experimental data, *Phys. Rev. C* **76**, 024309 (2007).
- [107] R. Jolos and E. Kolganova, Derivation of the Grodzins relation in collective nuclear model, *Phys. Lett. B* **820**, 136581 (2021).
- [108] M. Rudigier, J.-M. Régis, J. Jolie, K. Zell, and C. Fransen, Lifetime of the first excited 2^+ state in ^{172}W and ^{178}W , *Nucl. Phys. A* **847**, 89 (2010).
- [109] E. A. McCutchan and N. V. Zamfir, Simple description of light W, Os, and Pt nuclei in the interacting boson model, *Phys. Rev. C* **71**, 054306 (2005).
- [110] E. A. McCutchan, R. F. Casten, and N. V. Zamfir, Simple interpretation of shape evolution in Pt isotopes without intruder states, *Phys. Rev. C* **71**, 061301(R) (2005).
- [111] A. Harter, L. Knafla, G. Frießner, G. Häfner, J. Jolie, A. Blazhev, A. Dewald, F. Dunkel, A. Esmaylzadeh, C. Fransen, V. Karayonchev, K. Lawless, M. Ley, J.-M. Régis, and K. O. Zell, Lifetime measurements in the tungsten isotopes $^{176,178,180}\text{W}$, *Phys. Rev. C* **106**, 024326 (2022).
- [112] J. Wiederhold, V. Werner, R. Kern, N. Pietralla, D. Bucurescu, R. Carroll, N. Cooper, T. Daniel, D. Filipescu, N. Florea, R.-B. Gerst, D. Ghita, L. Gurgi, J. Jolie, R. S. Ilieva, R. Lica, N. Marginean, R. Marginean, C. Mihai, I. O. Mitu *et al.*, Evolution of $E2$ strength in the rare-earth isotopes $^{174,176,178,180}\text{Hf}$, *Phys. Rev. C* **99**, 024316 (2019).
- [113] N. Zamfir, G. Hering, R. Casten, and P. Paul, Hexadecapole deformations in actinide and trans-actinide nuclei, *Phys. Lett. B* **357**, 515 (1995).
- [114] J. Jolie and A. Linnemann, Prolate-oblate phase transition in the Hf-Hg mass region, *Phys. Rev. C* **68**, 031301(R) (2003).
- [115] D. Bonatsos, D. Lenis, D. Petrellis, and P. A. Terziev, $Z(5)$: Critical point symmetry for the prolate to oblate nuclear shape phase transition, *Phys. Lett. B* **588**, 172 (2004).
- [116] Y. Zhang, F. Pan, Y.-X. Liu, Y.-A. Luo, and J. P. Draayer, Analytically solvable prolate-oblate shape phase transitional description within the $SU(3)$ limit of the interacting boson model, *Phys. Rev. C* **85**, 064312 (2012).
- [117] T. Wang, B.-c. He, D.-k. Li, and C.-x. Zhou, Prolate-oblate asymmetric shape phase transition in the interacting boson model with $SU(3)$ higher-order interactions, *Phys. Rev. C* **107**, 064322 (2023).
- [118] J. A. Maruhn, P. G. Reinhard, P. D. Stevenson, and A. S. Umar, The TDHF code SKY3D, *Comput. Phys. Commun.* **185**, 2195 (2014).

- [119] B. Schuetrumpf, P. G. Reinhard, P. D. Stevenson, A. S. Umar, and J. A. Maruhn, The TDHF code SKY3D version 1.1, *Comput. Phys. Commun.* **229**, 211 (2018).
- [120] P. Alexa, M. Abolghasem, G. Thiamova, D. Bonatsos, T. R. Rodríguez, and P.-G. Reinhard, Macroscopic and microscopic description of phase transition in cerium isotopes, *Phys. Rev. C* **106**, 054304 (2022).
- [121] Hartree-Fock-Bogoliubov results based on the Gogny force, https://www-phynu.cea.fr/science_en_ligne/carte_potentiels_microscopiques/carte_potentiel_nucleaire_eng.htm (2006).
- [122] HFB+5DCH results, https://www-phynu.cea.fr/science_en_ligne/carte_potentiels_microscopiques/tables/HFB-5DCH-table_eng.htm (2006).